STRENGTHENING MECHANISMS IN FRICTION STIR ALLOYING OF AZ61 MAGNESIUM ALLOY AND MILD STEEL WITH Cu-CNT ADDITIVE

MOHAMMAD ASHRAF BIN ARIFFIN

FACULTY OF ENGINEERING
UNIVERSITI MALAYA
KUALA LUMPUR

2024

STRENGTHENING MECHANISMS IN FRICTION STIR ALLOYING OF AZ61 MAGNESIUM ALLOY AND MILD STEEL WITH Cu-CNT ADDITIVE

MOHAMMAD ASHRAF BIN ARIFFIN

DISSERTATION SUBMITTED IN FULFILMENT OF THE REQUIREMENTS FOR THE DEGREE OF MASTER OF ENGINEERING SCIENCE

FACULTY OF ENGINEERING
UNIVERSITI MALAYA
KUALA LUMPUR

2024

UNIVERSITI MALAYA

ORIGINAL LITERARY WORK DECLARATION

Name of Candidate: MOHAMMAD ASHRAF BIN ARIFFIN

Matric No: S2039234

Name of Degree: Master of Engineering Science

Title of Thesis: Strengthening Mechanisms in Friction Stir Alloying of AZ61 Magnesium Alloy and Mild Steel with Cu-CNT Additive

Field of Study: Engineering Design (NEC 521: Mechanics and Metal Work)

I do solemnly and sincerely declare that:

(1) I am the sole author/writer of this Work;
(2) This Work is original;
(3) Any use of any work in which copyright exists was done by way of fair dealing and for permitted purposes and any excerpt or extract from, or reference to or reproduction of any copyright work has been disclosed expressly and sufficiently and the title of the Work and its authorship have been acknowledged in this Work;
(4) I do not have any actual knowledge nor do I ought reasonably to know that the making of this work constitutes an infringement of any copyright work;
(5) I hereby assign all and every rights in the copyright to this Work to the Universiti Malaya ("UM"), who henceforth shall be owner of the copyright in this Work and that any reproduction or use in any form or by any means whatsoever is prohibited without the written consent of UM having been first had and obtained;
(6) I am fully aware that if in the course of making this Work I have infringed any copyright whether intentionally or otherwise, I may be subject to legal action or any other action as may be determined by UM.

Candidate's Signature Date: 29/12/2023

Subscribed and solemnly declared before,

Witness's Signature Date: 29/12/2023

Name:

Designation:

STRENGTHENING MECHANISMS IN FRICTION STIR ALLOYING OF AZ61 MAGNESIUM ALLOY AND MILD STEEL WITH Cu-CNT ADDITIVE

ABSTRACT

Dissimilar joining between lightweight magnesium (Mg) alloys and steel is essential to produce lighter vehicles, improve fuel efficiency, and reduce carbon emissions. However, the joining of Mg to steel is impractical due to the immiscible properties between these metals. In this experiment, friction stir alloying (FSA) with copper (Cu) and carbon nanotubes (CNT) additives is proposed to solve this problem. The additive, consisting of different wt.% of CNT in Cu powder was first added into the gap between the workpieces and then friction stir welding (FSW) was performed at varied traverse speeds and constant rotational speed. After the joining, microstructure characteristics and mechanical properties of Cu-CNT reinforced Mg-steel joints were investigated. Transmission electron microscopy (TEM) analysis of the Mg-steel joint revealed the formation of an intermetallic compound (IMC) at the interface of the joint. Further analysis by x-ray diffraction (XRD) showed a dominant presence of Mg_2Cu IMC, which indicated the interdiffusion of Cu into Mg element to establish the bonding. The presence of CNT inside the Mg matrix which was confirmed by TEM further contributed to the strengthening mechanism of the joint. Tensile and microhardness results revealed a notable enhancement of joint mechanical properties when Cu-CNT additive was added as compared to specimens with only Cu additive, and specimens without additive. The enhanced tensile strength and microhardness of the Cu-CNT reinforced Mg-steel joint was attributed to the dispersion of CNT inside the Mg matrix, which induced dislocations in the surface region, therefore improving the mechanical properties of the joint.

Keywords: friction stir alloying, friction stir welding, dissimilar joint, powder additives, carbon nanotubes, steel, magnesium alloy, copper powder

MEKANISME PENGUATAN DALAM PENGALOIAN KACAU GESERAN ANTARA MAGNESIUM ALOI AZ61 DAN KELULI LEMBUT DENGAN TAMBAHAN KUPRUM DAN TIUB NANOKARBON

ABSTRAK

Penyambungan bahan yang berbeza antara aloi magnesium (Mg) dan keluli adalah penting untuk menghasilkan kenderaan yang lebih ringan, meningkatkan kecekapan bahan api kenderaan dan mengurangkan pelepasan karbon. Walau bagaimanapun, penyambungan Mg kepada keluli adalah tidak praktikal kerana sifat tidak larut antara kedua-dua logam ini. Dalam eksperimen ini, pengaloian kacau geseran (PKG) dicadangkan untuk menyelesaikan masalah ini. Bahan serbuk tambahan, yang terdiri daripada peratusan berat tiub nanokarbon (TNK) yang berbeza di dalam serbuk kuprum, (Cu) ditambah di antara aloi Mg dan keluli sebelum proses kimpalan kacau geseran (KCG) dijalankan pada kelajuan yang berbeza-beza. Selepas penyambungan, ciri-ciri struktur mikro dan sifat mekanikal penyambungan antara Mg dan keluli yang ditambah Cu-TNK telah dianalisa. Analisis mikroskop elektron penghantaran (TEM) terhadap sambungan Mg-keluli mendedahkan pembentukan sebatian antara logam di antara permukaan sambungan. Analisis lanjut oleh difraksi sinar-X (XRD) menunjukkan kehadiran dominan komponen Mg2Cu yang menunjukkan interdifusi Cu ke dalam Mg untuk mewujudkan ikatan antara logam. Kehadiran TNK di dalam matrik Mg juga disahkan oleh TEM yang menyumbang kepada kesan pengukuhan sambungan. Keputusan kekuatan dan kekerasan mikro menunjukkan peningkatan ketara pada sifat mekanikal apabila serbuk Cu-TNK ditambah berbanding spesimen dengan hanya bahan tambahan Cu, dan spesimen tanpa bahan tambahan. Kekuatan dan kekerasan mikro yang dipertingkatkan pada sambungan Mg-keluli melalui tambahan Cu-TNK adalah disebabkan oleh penyebaran TNK di dalam Mg, yang menyebabkan pelbagai kehelan di kawasan permukaan, oleh itu menambah baik sifat mekanikal penyambungan tersebut.

Kata Kunci: Pengaloian kacau geseran, kimpalan kacau geseran, sambungan tidak serupa, bahan tambah serbuk, tiub nano karbon, keluli, aloi magnesium, serbuk tembaga

ACKNOWLEDGEMENTS

I would like to express my gratitude to my supervisors, Dr. Mohd Ridha Bin Muhamad and Associate Prof. Dr. Farazila Binti Yusof for their advice and guidance from the very start this work as well as for giving me extraordinary experiences throughout the work. The extensive discussions around my work and interesting exploration in difficult concepts have been very helpful for this study. I am indebted to them more than they know.

Besides, I would like to acknowledge the Universiti Malaya, Malaysia and Joining and Welding Research Institute (JWRI), Osaka University, Japan for providing the necessary facilities and resources for this research. I would also like to thank all the research group members, especially Dr. Sufian Raja, Mohammad Syahid, and Muhammad Zulhiqmi for their endless support and cooperation in the success of this research. Not to forget, the assistant engineers from Mechanical Engineering Department of University Malaya, Mr. Mohd Fauzi Bakri, Mr. Nasrizam Mohamed and Mrs. Hartini Baharum for their contributions and support in specimen preparation for experimental works and analysis.

This research is supported by the Research University Grant Scheme (No. GPF062A-2020, GPF062B-2020).

TABLE OF CONTENTS

LIST OF FIGURES

LIST OF TABLES

LIST OF SYMBOLS AND ABBREVIATIONS

CNT	:	Carbon nanotube
EDS	:	Energy dispersive X-ray
FESEM	:	Field emission-scanning electron microscopy
FSA	:	Friction stir alloying
FSP	:	Friction stir processing
FSLW	:	Friction stir lap welding
FSSW	:	Friction stir spot welding
FSW	:	Friction stir welding
IMC	:	Intermetallic compound
OM	:	Optical microscope
RSW	:	Resistance spot welding
SAED	:	Selected area electron diffraction
TEM	:	Transmission electron microscopy
TIG	:	Tungsten inert gas
USW	:	Ultrasonic spot welding

CHAPTER 1: INTRODUCTION

The rise in carbon dioxide (CO_2) levels and other greenhouse gases in the atmosphere is affecting the global temperature and air quality in every continent. A report published by Ritchie & Roser (2020) from Our World in Data presented that the energy sector accounted for approximately 70% of greenhouse gas emissions which mainly contributed by transportations, buildings, and unallocated fuel combustion. United Nations Framework on Climate Change Convention reported that the transportation alone contributed 27% of greenhouse gas emissions in the US and almost 30% of emissions in european countries, which believe to be one of the major causes of the greenhouse effect worldwide (Massar et al., 2021). The rising amount of pollution and greenhouse gases emissions can be reduced significantly by improving the fuel efficiency of vehicles.

One approach to improve the vehicle's fuel efficiency is by minimizing the vehicle's weight. A research by Serrenho et al. (2017). suggested that fostering vehicle weight reduction yielded to more fuel effeciency and greater cumulative emissions savings than speeding up the transition to electric drivetrains. Figure 1.1 below shows the relationship between car mass and fuel efficieny, which explains that the fuel effeciency is increased when the car mass is reduced.

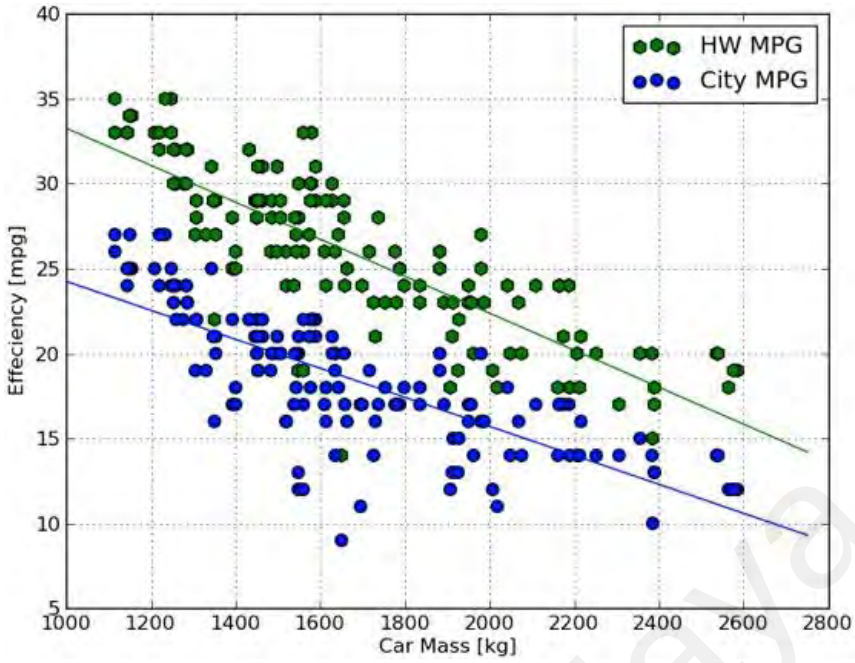

Figure 1.1: Relationship between mass of car and fuel efficiency (Serrenho et al., 2017)

Weight reduction also could produce greater savings in manufacturing cost when conventional material in the car body is substituted with low-cost, lightweight, and high-strength materials (Mayyas et al., 2016). Material substitution of light metals such as magnesium and aluminium alloys for steel can effectively reduce the vehicle body weight, improve fuel consumption, and produce less carbon (Ogawa et al., 2016). In many engineering applications, steel has been the primary choice of material owning to its superior strength and low cost. In fact, parts of the vehicle structures such as body frame and engine cradle require materials with high strength and toughness in which the properties could be achieved by the use of steel. A potential solution to reduce the overall weight of the component is by using dissimilar joints to substitute parts of the steel structures with lighter materials on the parts where high strength properties are not required.

Magnesium alloys have been recognized as a potential material for dissimilar joints as they exhibit excellent mechanical properties. Magnesium tensile strength is close to that

the strength of aluminium but it is 33% lighter (X. Cao et al., 2006). Newly developed magnesium alloys such as the AZ (Aluminum and Zinc) family which includes AZ31, AZ61, and AZ91E have already been adopted in a vast spectrum of applications especially in the aircraft and automotive industries (Dziubińska et al., 2016). For example, aircraft and automotive industries use a wide range of magnesium alloy parts from instrumental panels to seat components and engine parts (Gwynne & Lyon, 2007; Kulekci, 2008). Such applications of Mg alloys in aircraft and automotive designs enables weight reduction of the overall vehicle mass and thus reduces fuel consumption. Although more and more parts are made of Mg alloys, the joining of Mg alloys to primary metal like steel remains to be a significant barrier to greater adoption of the material in industries. Therefore, effective techniques for joining lightweight magnesium and steel must be developed to achieve successful dissimilar joints between Mg and steel. In many literatures, friction stir welding (FSW) was reported as a promising technique for joining dissimilar materials (Akinlabi, 2010; Kumar et al., 2015; Song et al., 2018). FSW is a solid-state welding process in which the interfacial reaction between base materials occurs below their melting temperature. The process involves a non-consumable rotating tool which is plunged into the adjacent edges of metal sheets and traverses along the joint line. Frictional heat is generated as a result of the stirring action between rotating tool and the workpieces, which then soften the materials being welded and form the joint (Singh et al., 2019). Numerous researches have reported the success of FSW in joining dissimilar materials (bin Muhamad et al., 2021; Kasai et al., 2015; Schneider et al., 2011; Singh et al., 2019). Besides, major automitve industries have successfully implemented the use of FSW to manufacture sub-frame structures from dissimilar materials (Kusuda, 2013; Meyer, 2012). Not only in automotive industry, FSW also provides many advantages to various manufacturing sectors for a wide range of applications. However, joining immiscible materials especially Mg and steel is difficult to obtain high-quality joints

because they inhibit the development of an intermetallic compound (IMC) at the interface. To overcome the immiscibility issue, filler or additive materials are used in dissimilar joining and have drawn a lot of attention recently since it can help to promote metallurgical reaction between the weld materials. Friction stir alloying (FSA), which derives inspiration from FSW is by far a promosing technique for joining dissmilar materials by means of employing additive materials at the joint interface. In FSA, metal particles are incorporated within the workpiece metals as alloying materials for better metallurgical reaction between the materials to promote properties improvement of dissimilar joints. To date, FSA has reported its success in fabricating metal-matrix composites, homogenising powder metallurgy processes, as well as the formation alloyed joints (Raja et al., 2022; Sharma, et al., 2020). In addition, extended research must be conducted to fully utilize the advantage of FSA in producing dissimilar joints. Therefore this research proposed that the joint properties of Mg alloy and steel can be further enhanced using FSA process by adding Cu-CNT powder additives as reinforcement materials. Because of low solid solubility of steel in Mg, the addition of Cu would reduce the immiscibility gap and facilitate the formation of intermetallic compound (IMC) at joint interfaces. The formation of IMC indicates the presence of metallurgical bonding between Mg and Fe, which gives strengthening effect to welded joints. It is also expected that the incorporation of CNT would promote interfacial bonding between CNT and the interface region that further reinforces the Mg-steel joint strength.

1.1 Problem Statement

The joining of Mg to steel is important to meet the demand for lightweight, fuel-efficient, and low carbon emissive transportations. However, joining dissimilar materials is challenging due to various metallurgical concerns. Firstly, Mg and steel are immiscible, such that the maximum solubility of steel in Mg is only 0.00041 wt.% (Okamoto & Massalski, 1990). In addition, steel and Mg have vast differences in mechanical and

thermal properties, which limits the use of conventional welding techniques like fusion welding or tungsten inert gas (TIG) welding (Jana et al., 2010). Besides, FSW between Fe and Mg hardly results in the formation of IMCs due to the immiscibility of these elements, which means both metals hardly react with each other to form a joint. Implying mechanical joining methods to produce dissimilar materials joint is not preferable as there exist several disadvantages such as low joint strength and weak fatigue performance due to the absence of metallurgical bonding (Yan et al., 2017). Futhermore, dissimilar joint via conventional welding techniques involve melting of materials which is likely to produce defective welds such as voids, porosity, and cracks (L. Liu et al., 2010). In the context of joining, mettalurgical bonding is the type of bonding which involves interdiffusion of atoms at the interface of metal workpieces to form unified joints. (He et al., 2019). When joining dissimilar materials, metallurgical bonding is favored for its ability to create IMC layer, which enhances the joint properties between the two metals (Xue et al., 2010). The formation of IMC requires some specific conditions to take place such as eleveted temperature and high pressure to facilitate the diffusion of metal atoms which is known as metallurgical reaction. A study about joining phenomenon of friction stir welded Al/Fe joints suggested the metallurgical reaction took place when Al, Fe, and Cr diffused at the weld interface and formed an IMC layer (Y. Liu et al., 2020). Several researches to join dissimilar materials between Mg and steel using FSW have been conducted. In an earlier attempt, low carbon steel was used to join with AZ31 Mg alloy using FSW however no joint was produced between the weld materials due to the absence of metallurgical reaction (Chen & Nakata, 2010). In another research, FSW between low carbon steel with different type of Mg alloys reported that better joint performance was obtained when the aluminium content in the Mg alloys was increased (Kasai et al., 2015). The increase in the joint mechanical properties was contributed by the formation of Al-Fe IMC at the joint interface. However, the consturction of Al-Fe IMC caused the

depletion of Al content in the Mg side near the interface which affected the tensile strength of Mg-steel joint. To resolve this, an Al powder was added in between the butt surfaces of Mg alloy and steel workpieces (bin Muhamad et al., 2021). SEM-EDS of the Al-added Mg-steel joint showed that the Al content in the vicinity of joint interface was successfully maintained. However, the selection of Al as the interlayer additive prompted the formation of Al-Mg layer in adjacent to Al-Fe IMC layer (X. Y. Wang et al., 2016). The joining of these IMCs became a weak link to the interface, which determined the interface strength as it would break first when subjected to tensile test. Therefore, the types of reinforcing material at the interface play a vital factor in determining the strenght and other properties of the joint.

In summary, the low solubility of solid Mg in Fe, vast differences in thermal properties, and the absence of metallurgical reaction between Mg and Fe are the primary challenges that need to be addressed when joining Mg alloy to steel. The introduction of compatible metal powders in between the dissimilar weld materials would solve the immiscibility issue, but must be carefully selected as it has great influence towards the joining strength.

1.2 Research Objective

This study aims to produce dissimilar joint between AZ61 Mg alloy and mild steel using FSA and to investigate the joint mechanical properties, its microstructural evolution at the interface, and the joining mechanism involved. The specific objectives of the research are as follows:

1. To investigate the effect of traverse speed and CNT powder additives on the mechanical properties of the Mg-steel joint produced by FSA

2. To assess the Mg-steel joint quality at microstructural level and joining mechanisms involved such as metallurgical bonding and interfacial reactions that could contribute to the joining strength.
3. To evaluate the role of Cu powder in facilitating the construction of the intermetallic compound at Mg-steel joint interface.

1.3 Scope and Significance of the Research

This research focuses on the effect of copper and CNT powder additives on the microstructures and mechanical properties of Mg-steel joint produced by FSA. Butt joints between Mg and steel will be produced by using 5 different additive conditions at the joint interface. Every experimental condition will be conducted at 3 different traverse speeds while keeping other parameters constant. Mechanical properties for all of the joint specimens will be evaluated based on tensile analysis and only the specimen with the highest tensile result will be used for detailed microstructure analysis. Microstructure analysis in this research will be done to identify the effect of copper and CNT powder additives on the joining mechanisms and possible strengthening mechanisms that contributes to improved tensile strength. The analysis will not extend to the advanced factors that affect the joint properties such as the properties of IMC and detailed metallurgical reactions that occur during the FSA process.

The research is essential for both researchers and manufacturers to gain a thorough understanding of the mechanisms behind the joining of magnesium alloy and steel. In addition, welding engineers could use the outcomes of this study to develop magnesium alloy and steel reinforced FSA joints with superior mechanical properties. Besides, this research could serve as a guide for automotive manufacturers to consider implementing reinforced FSA technique as part of the manufacturing processes for joining magnesium alloy and steel components.

1.4 Thesis Structure

The thesis is divided into five chapters. The first chapter provides an introduction to the topic and states the problems and the objectives of the research.

Chapter two describes the background of FSW and FSA of magnesium alloy and steel. This chapter also discusses the established research and studies regarding the effect of the reinforcing materials on the performance of the joint and the research gap that needs to be addressed.

Chapter three presents the list of materials, the experimental methods, and the types of analysis used in this research.

Chapter four describes the experimental results, with details discussion on the effect of reinforcement additive towards the mechanical properties of the joint and its microstructural features.

Finally, chapter five provides conclusions of the results and recommendations for future work.

CHAPTER 2: LITERATURE REVIEWS

The effective joining of dissimilar materials between Mg and steel is significant for harnessing the lightweight properties of Mg and the strength of steel to produce lighter and more reliable vehicle structures. This chapter begins by discussing the importance of Mg-steel joining and exploring the existing joining methods for Mg and steel. A substantial portion of the literature review is dedicated to the fundamentals of FSW, which has gained popularity for its ability to overcome the difficulties associated with traditional welding methods. Discussion on the fundamentals of FSW includes the understanding of FSW principles and its critical process parameters. The chapter extends to discussion on formation of IMC in dissimilar joining and reinforcement materials in FSW/FSA, which analyzes the types of reinforcement materials employed and their impact on the joint's performance.

In essence, this chapter serves as a comprehensive study of Mg-steel joining in order to understand recent research progress in the field of dissimilar joining and identify the current research gap, in which will be utilized for achieving the objectives of the present study.

2.1 Importance of Magnesium Alloy and Steel Joining and Its Challenges

The growth in fossil fuel consumption and the decline in hydrocarbon supply necessitates the development of innovative technologies to counteract the issue. Around 70% of fossil fuel usage in the US is attributed to transportation, including automobiles, trucks, and buses (Vallentin, 2008). Statistics from the United Nations Framework on Climate Change Convention in 2018 reported that the transportation sector in the United States was responsible for over 30% of the country's energy-related CO_2 emissions (Massar et al., 2021). Reducing structural weight of the vehicles can effectively improve the fuel comsumption, thus mitigating high carbon emissions from the transportation

sector. A study shows that a 100 kg weight loss in vehicles can result in a 20 g/km CO_2 reduction (Ishikawa et al., 2018). In addition, a 10% reduction in vehicle weight can lead to 5% increase in fuel efficiency (Serrenho et al., 2017). In automotive manufacturing, primary metal material, which is steel, accounts for over 50% of the weight of the average vehicle (Horton & Allwood, 2017). Therefore, substituting parts of the steel structure with lighter structural material is a promising method to reduce the weight of the vehicle.

Lighter materials such as aluminium alloys, magnesium alloys, and carbon fibre polymer composites have been used by researchers to substitute a part of steel components in cars (Kawajiri et al., 2020). The ideal material substitution must have a high strength-to-weight ratio and be capable of forming a strong joint with the existing steel components. Carbon fibre polymer composites have a greater specific strength at relatively lower density than aluminium alloys and magnesium alloys, however their tolerance to high temperatures is lower than metals (Van Acker et al., 2009). Magnesium alloys appear to be a better option as a dissimilar joint material than aluminium alloys since they are nearly as strong as aluminium, but 33% lighter. While magnesium alloys provide better lightweight advantage over other structural metal materials, there exist several unique challenges in forming a strong joint between magnesium and steel.

First, the joining of Mg to steel is challenging due to the significant differences in their thermal and mechanical characteristics (Jana et al., 2010). The characteristics of steel and magnesium are summarized in Table 1 below.

Table 1: Thermal and mechanical properties of steel and pure magnesium (Song et al., 2018)

Properties	Magnesium	Steel
Melting point (°C)	650	1536
Boiling point (°C)	1.09×10^3	2.860×10^3
Thermal conductivity (W·m−1·K−1)	78	38

Coefficient of thermal expansion (1/K)	2.5 x 10^{-5}	1 x 10^{-5}
Density (kg·m−3)	1.59 x 103	7.02 x 103
Young's modulus (GPa)	45	211

Because of the huge variations of properties between steel and magnesium, the joint between these materials experiences immiscibility, which makes conventional joining methods difficult. Second, according to Mg-Fe binary phase diagram as shown in Figure 2.1, there is almost zero solubility of Mg in Fe and also no intermetallic phases can be formed between Mg and Fe (Guo et al., 2009). As a result, the dissimilar joint between pure Mg and steel leads to weakened joint strength due to the absence of metallurgical bonding (R. Cao et al., 2017).

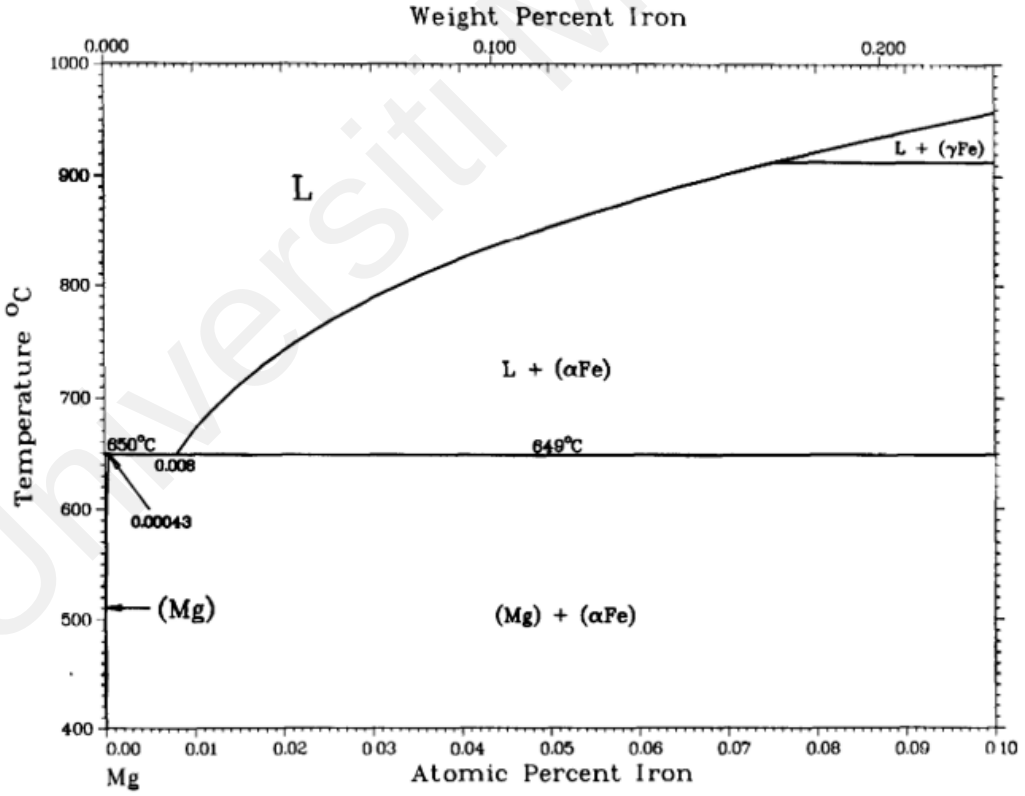

Figure 2.1: Mg-Fe binary phase diagram (Okamoto & Massalski, 1990)

2.2 Joining Methods between Magnesium Alloys and Steel

Despite the challenges, researchers have applied various joining methods such as fusion welding and solid-state welding to join Mg to steel. Several fusion welding techniques that have been used are hybrid laser and tungsten inert gas (TIG) welding, laser brazing welding, laser welding, and resistance spot welding (RSW) (L. Liu et al., 2010; Qi & Liu, 2012; X. Y. Wang et al., 2016). Apart from that, solid-state joining methods like friction stir welding (FSW), friction stir spot welding (FSSW), and ultrasonic spot welding (USW) are also gaining popularities among researchers to produce Mg-steel joints (Kasai et al., 2015; Liyanage et al., 2009; V. K. Patel et al., 2013).

2.2.1 Fusion Welding

Fusion welding is a welding technique where the joint is formed by melting and solidifying the weld materials. A filler can be used to improve joint characteristics and compensate for variations in the weld materials composition. Laser beam welding is one of the fusion welding techniques, which employes a laser beam to melt the joining surfaces. A laser beam welding was conducted to join AZ31 Mg alloy and low carbon steel by allowing the Mg alloy to melt while restricting the melting of steel (Miao et al., 2010). In the experiment, the molten Mg alloy acted as a filler metal that formed a joint with the solid steel by wetting and diffusing. Upon SEM analysis, a Mg-Fe transition-layer was discovered due to the strong diffusion interaction between molten Mg alloy and solid steel as observed in Figure 2.2(a). The fracture of the laser beam joint occured at the joint interface and its average tensile strength reached up to 182 MPa. It was mentioned that the key parameters controlling the thickness of the transition layer are the melting time and the absolute temperature of the interface. However, the influence of the thickness of transition layer on the tensile strength was not discussed in the study.

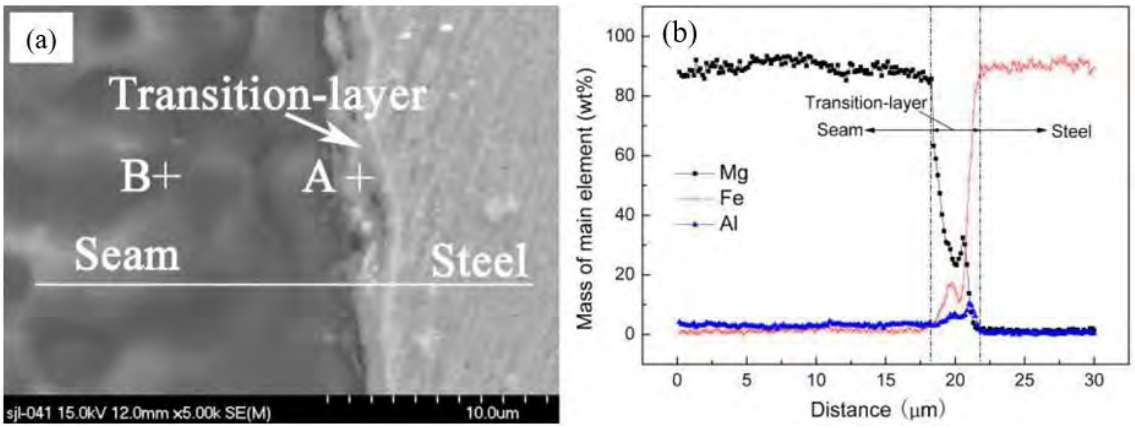

Figure 2.2: Interface characteristics of Mg-steel joint (a) Mg-Fe transition layer and (b) elemental distribution at interface (Miao et al., 2010)

Since the joining between dissimilar materials is impaired by the differences in their thermal properties and poor metallurgical compatibility, a laser offset welding was performed between AZ31B Mg alloy and 316 stainless steel, in which the laser beam was focused on the top surface of the steel side at an offset distance from the joint interface (Casalino et al., 2017). The offset was employed in the process to avoid mixing of liquid phases of both metals which could weaken the joint properties. By using this method, high melting point metal was first melted and then wetted the low melting point metal through heat propagation, hence forming a joint. A schematic diagram that described the joining mechanicsm of the technique is shown in Figure 2.3.

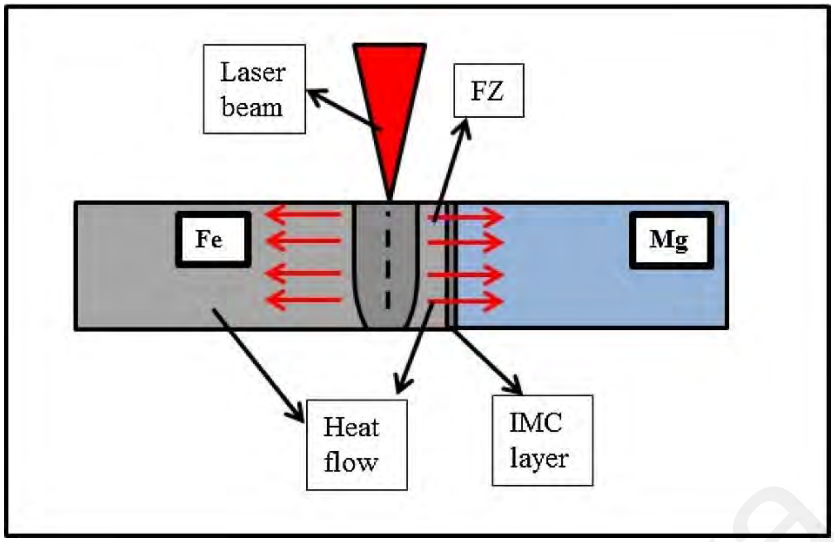

Figure 2.3 Schematic diagram of joining mechanism by laser offset welding technique (Casalino et al., 2017)

The method demonstrated a promising capability in joining dissimilar metal welds, which achieved a joint tensile strength of more than 100 MPa. The strength of the joint was attributed to the formation of thin intermetallic layer within the fusion zone as revealed by the SEM analysis in Figure 2.4.

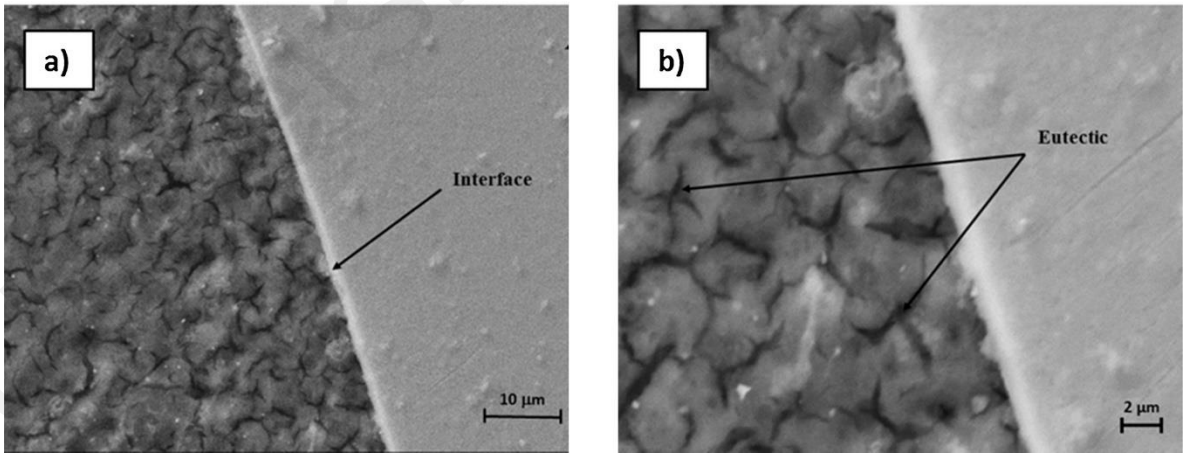

Figure 2.4 (a) Mg-steel interface and (b) evidence of eutectic formation and intermetallic layer (Casalino et al., 2017)

Besides, the joint specimens demonstrated a tensile fracture in the Mg side, which indicates the effectiveness of the interface. From metallurgical point of view, it is not possible for pure Mg to form sollid state diffusion with Fe. To overcame that, an Al

interlayer was used during laser welding between AZ31 and steel to enhance metallurgical reaction at the interface (C. W. Tan et al., 2016). SEM analyis of the joint interface as shown in Figure 2.5 showed that the metallurgical bonding between Mg and steel was formed, which resulted from the dissolution of the Al interlayer into the Mg fusion zone and mutual diffusion with steel. In addition, varied thicknesses of Fe-Al interlayer was also formed along the fusion zone-steel interface when different Al interlayer thickness was used.

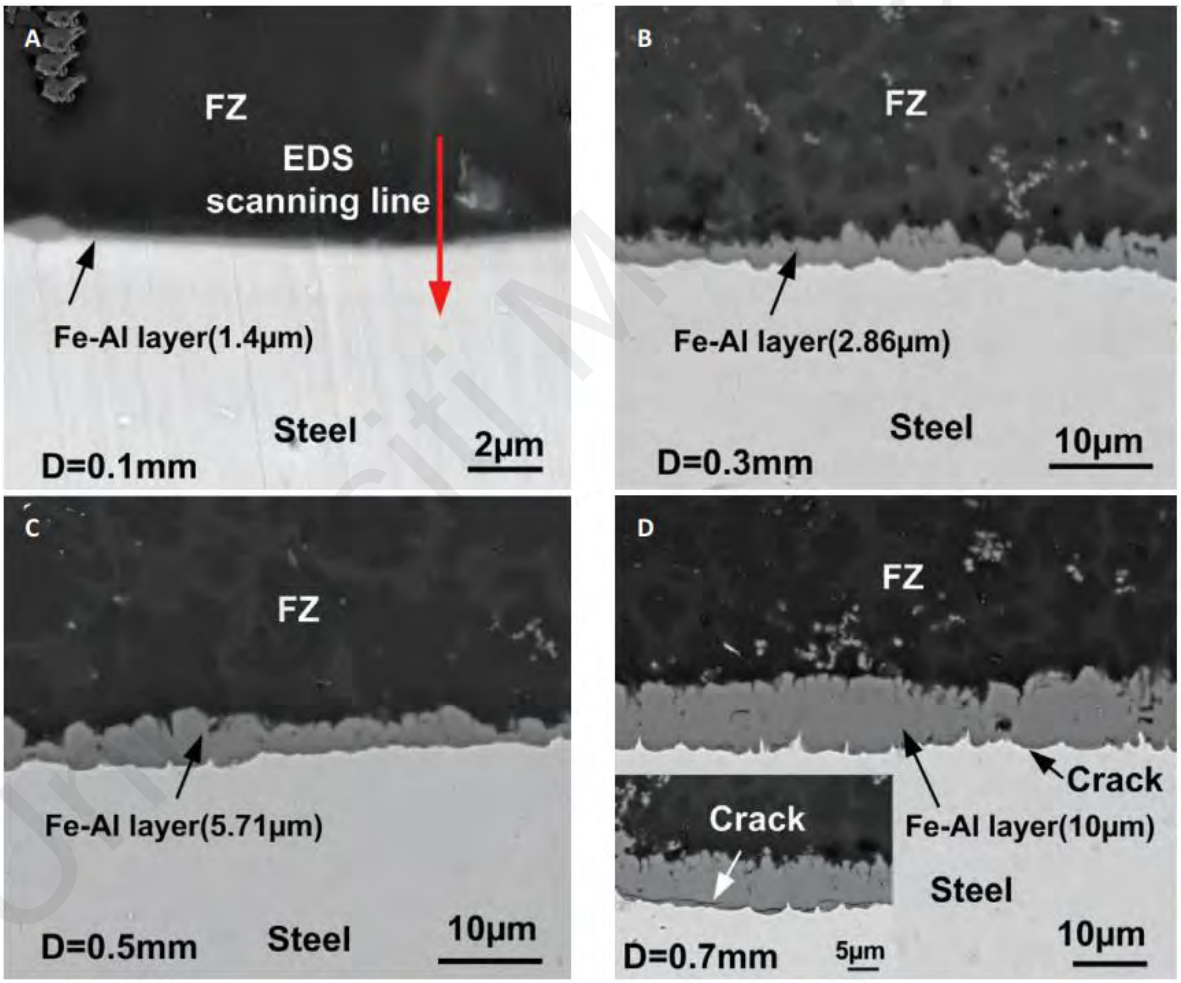

Figure 2.5 SEM images of Mg-steel welded interface with different thickness of Al interlayers (a) 0.1, (b) 0.3, (c) 0.5, and (d) 0.7 mm (C. W. Tan et al., 2016)

When the Fe-Al interlayer was lesss than 2 μm, Fe(Al) solid solution and the $Al_8(Mn, Fe)_5$ phase was developed next to the steel interface, whereas the Al_6Fe phase was formed when the reaction layer was more than 2 μm thick. The highest recorded value of the

tensile-shear fracture load was 133 N/mm, which corresponded to a joint efficiency of 40.3% with respect to the steel base metal. An increase in the interfacial layer, however, led to increased amounts of brittle MgAl compounds and interface cracking, which reduced the joint mechanical properties.

Laser-tungsten inert gas (TIG) hybrid welding was developed for connecting Mg alloys to Zn coated steel in lap joint configuration (C. Tan et al., 2013). With this method, the tensile-shear strength reached a maximum of 68 MPa, indicating 52.3% joint efficiency in comparison to Mg base metal. It was reported that the Al element in AZ31B Mg alloys diffused to the liquid/solid interface and reacted with Fe and Mn elements from steel, resulting in the metallurgical bonding at the interface. The interfacial failure was caused by the poor bonding between the Mg-Zn reaction layer and the newly created Fe-Al layer. To promote metallurgical reaction between Mg and steel, researchers have applied various types of metal interlayers that could interact with both Mg and Fe elements. In a study, different types of interlayers, Cu and Ni, were added when joining Mg alloy and mild steel using the hybrid laser-TIG welding technique (L. Liu & Qi, 2010). The tensile results revealed that the shear strength of the Cu-added joint was somewhat greater than that of the Ni-added joint. SEM examination on the fracture surfaces as depicted in Figure 2.6 showed that fracture surface of the Ni-added joint has greater torn, larger smooth areas, and plenty of tiny pits, indicating that the joint demonstrated certain plasticity. The fracture surface of the Cu-added joint, on the other hand, has a high number of fine arrises and pits with no smooth areas or huge arrises, showing that the plasticity of the Cu-added joint is better than that of the Ni-added.

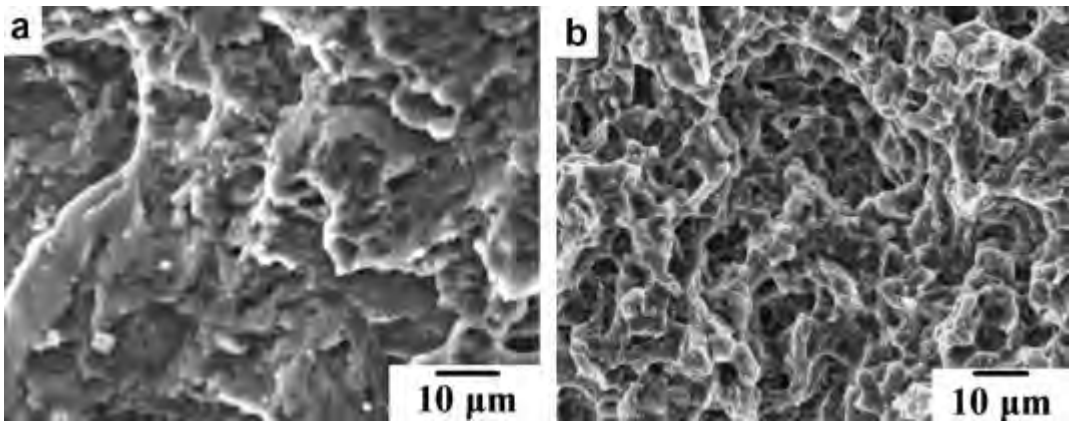

Figure 2.6: SEM images of fracture surface of (a) Ni-added joint and (b) Cu-added joint (L. Liu & Qi, 2010)

However, the welded joints produced by these techniques are unable to avoid defects such as porosity, voids, and cracks as shown in Figure 2.7(a) (L. Liu et al., 2010; Qi & Liu, 2012). Recently, resistance rivet welding was carried out on Mg and Fe where high heat input was generated through resistance to melt both materials to form metallurgical-mechanical hybrid joints. However, the differences in thermal properties has caused nonsynchronous solidification process of Mg and Fe to occur, which leads the formation of hollow sphere weld as illustrated in Figure 2.7(b) (Niu et al., 2021).

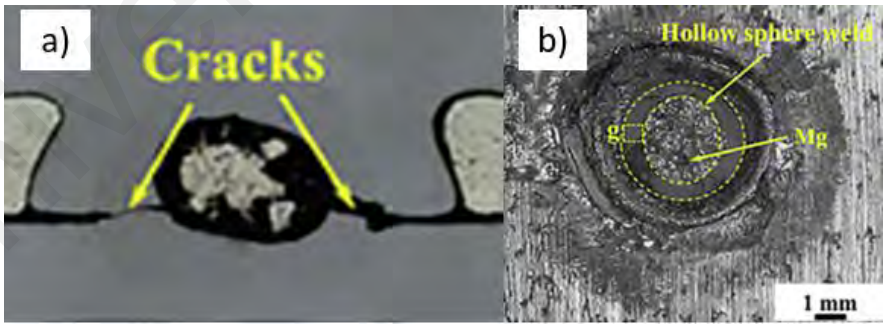

Figure 2.7: (a) Cracks and (b) hollow sphere defects between dissimilar Mg-steel joint (Niu et al., 2021)

2.2.2 Diffusion Bonding

Diffusion bonding is a solid-state joining technique which commonly use to join dissimilar materials like magnesium and steel. Various solid-state joining technique have been applied for joining Mg alloys to steel such as ultrasonic spot welding (USW), friction

stir spot welding (FSSW), and friction stir welding (FSW). Since it is a solid-state technique, the process does not involve the melting of weld materials, avoiding the formation of post-weld defects as seen in the fusion welding techniques (Casalino et al., 2017; Qi & Liu, 2012). Besides, the differences in physical and metallurgical properties between steel and Mg encounter many limitations when using conventional fusion welding methods. In an attempt to overcome the said limitation, 316L stainless steel and AZ31 Mg alloy were joined using diffusion bonding method with the help of Cu and Ni interlayers to achieve good contact between the bonded interfaces (Elthalabawy & Khan, 2011). The Mg-steel joint achieved a shear strength value of 57 MPa when joining with Cu interlayer meanwhile the joint resulted in a strength value of 32 MPa when joining with Ni interlayer. Both Cu and Ni interlayers formed a eutectic phase with Mg and the formation of stable intermetallic phases improved the hardness within the joints. V. K. Patel et al. (2014) in the ultrasonic spot welding (USW) of Mg to galvanized and ungalvanized steel studied the effect of the Sn interlayer on the microstructure and mechanical properties of the dissimilar joints. It was found that a weak joint occurred in the welded Mg to ungalvanized steel since Mg and Fe elements were unable to react with each other. On the other hand, The tensile shear strength of Mg and ungalvanized steel joint increased significantly with the addition of Sn interlayer. The improvement was attributed to the generation of solid solutions of Sn with Fe and Mg together with the Mg_2Sn composite in the joint interlayer.

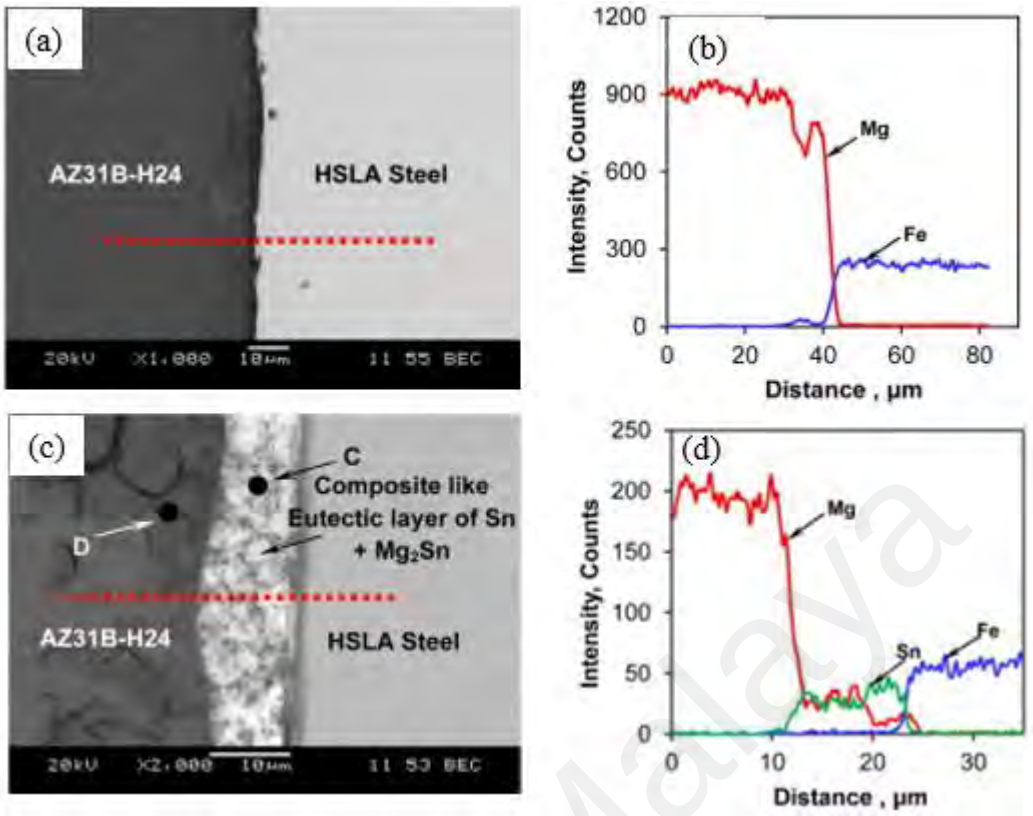

Figure 2.8: SEM micrograph at the center of USWed Mg to steel joint (a) without Sn interlayer, (c) with Sn interlayer, and their respective EDS line scan across the interface (b) and (d) (V. K. Patel et al., 2014).

Based on the SEM micrograph shown in Figure 2.8(a), it can be observed that the transitional layer between Mg and steel was not detected, meanwhile a composite-like eutectic layer of Sn and Mg_2Sn was observed at the center of weld zone as displayed in Figure 2.8(c). EDS line scan of the image revealed that elemental composition at point C consisted of 70% Mg and 30% Sn, suggesting that only Mg and Sn elements were present in the joint interlayer. In addition, little or no Fe was detected across the interface. This was due to the greater solubility of Sn in Mg than the solubility of Sn in Fe.

Zn coated steel was also used in the solid-state welding of dissimilar Mg to steel and the joints demonstrated better mechanical properties than the joints made with uncoated steel (Chen & Nakata, 2010). It was reported that the friction stir welded of AZ31 Mg alloy to Zn coated steel achieved greater failure loads than the welded Mg alloy to bare steel. This is because the presence of Zn coating promoted the formation of Mg-Zn

intermetallic products at the joint interface, improving the weldability between the weld materials.

2.3 Joining Mechanism of Magnesium and Steel

According to the past studies on the different joining techniques to join dissimilar materials like Mg and steel, it can be summarized that the main joining mechanism responsible for joining Mg with steel is the metallurgical bonding between weld materials. Reactive alloying elements in Mg alloys such as Al and Zn facilitates the joinability between Mg and steel through the formation IMC (T. Wang et al., 2019). Besides, metallurgically miscible interlayers such as Zn, Al, and Cu also facilitates the formation of solid solution or IMC layer between the Mg matrix which further strengthen the bonding at the joining interface (bin Muhamad et al., 2021; Hou et al., 2021; C. W. Tan et al., 2016; X. Y. Wang et al., 2016).

Many literatures reported that the joining between Mg and steel tend to be weak or unbonded when no interlayer or coating is used (Chen & Nakata, 2010; DQ et al., 2015; Kasai et al., 2015). This is due to the fact that Mg and Fe are metallurgically incompatible, and metal oxides on the Mg surface prevent metallurgical reaction between Mg alloys and steel. With interlayers, the immiscibility gap between dissimilar materials can be reduced, by promoting the formation of solid solution and IMCs at the joining interface. Lately, studies on the joining of immiscible magnesium to steel focuses mostly on reducing the immiscibility gap between the materials by utilizing base metal alloying elements and suitable metal additves to generate IMC features. Therefore, it is crucial to produce a metallurgical bond for joining immiscble materials like steel and Mg. This can be achieved by enhancing interfacial reaction between Mg and steel through secondary reinforcing elements to promote the formation of IMC.

A promising joining method to metallurgically bond Mg with steel and obtain a sound joint is by implying FSW technique. The joining of dissimilar metals using FSW is achieved by severe plastic deformation which allows the flow of plasticized materials occurring in solid state (T. Wang et al., 2021). Since the invention of FSW, the method has been continually improved and its range of application has been expanded. An example of innovative application of FSW was demonstrated by Mishra et al. in which friction stir processing (FSP) was developed based on the FSW basic principles to produce surface composite and surface modification of metal matrix composites (R. S. Mishra & Ma, 2005). In their work, Al-SiC surface composites were successfully fabricated by uniformly distributing the SiC particles in the Al matrix via FSP, producing fine microstructure in the stir zone that resulted in high performance of surface composites. Basing on the basic principles of FSW and FSP, a new generic joining technique, friction stir alloying (FSA) was developed for fabricating composite or alloyed joints. In the early research of the composite joints fabrication, SiC nanoparticles was employed as reinforcement particles when joining pure Cu plates using FSA technique (Bahrami et al., 2014; Sun & Fujii, 2011). The studies reported that SiC added joints showed remarkably improved tensile strength and microhardness due to the pinning effect of SiC, hindering the grain growth after severe plastic deformation, therefore enhancing the joint mechanical properties.

Although FSW and its derivatives are relatively new solid-state processing technique, the process already exhibits a considerable enhancement in strength and microhardness as compared to conventional fusion welding. In the following section, the fundamentals of FSW and its development were addressed. The discussion will be emphasized on FSW process parameters, joining of Mg and steel using FSW, the development of FSA, and nanomaterials reinforcement in FSW and FSA.

2.4 Fundamentals of FSW

Friction Stir Welding (FSW) is a solid-state joining process developed by The Welding Institute Ltd in 1991. FSW operates by rotating and plunging a non-consumable tool into the surface of two workpieces. The plunged tool then travels along the joint line, causing the material to heat up and plasticized due to frictional heat. Through frictional heating and severe plastic deformation, the rotating tool mechanically mixes the plasticized materials and hence, join the two workpieces together. General schematic of the FSW process is illustrated in Figure 2.9 below (Gibson et al., 2014).

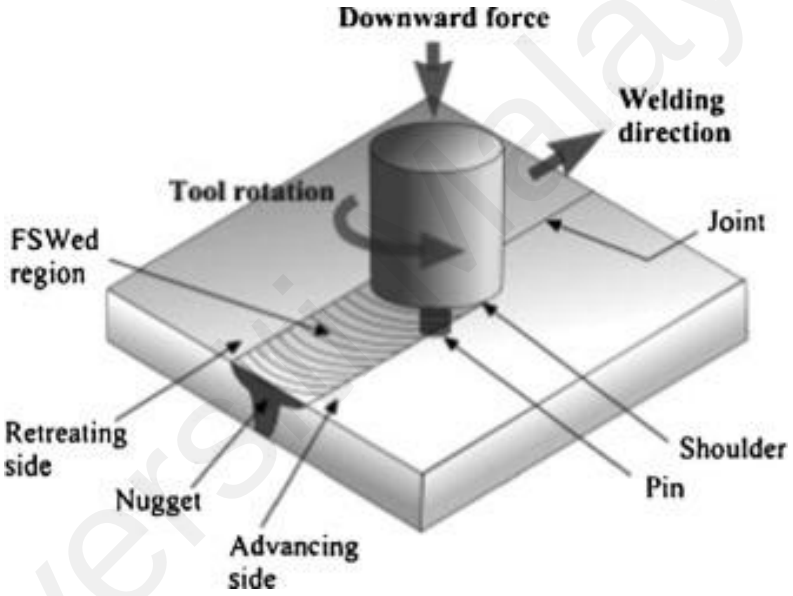

Figure 2.9: Basic schematic diagram of the FSW process (Gibson et al., 2014)

FSW has shown great success in joining dissimilar materials, according to numerous studies (bin Muhamad et al., 2021; Kasai et al., 2015; Schneider et al., 2011; Singh et al., 2019). In addition, major automotive players have successfully implemented the use of FSW in manufacturing sub-frame structures from dissimilar materials (Kusuda, 2013; Meyer, 2012). Not only in automotive industry, FSW has also received a lot of scientific and technological attention in various industries including aircraft, railroad, and renewable energy (Gibson et al., 2014; T. A. Patel & Badheka, 2022). To assure the structural integrity, safety, and service life of the fabricated products, research to address

inherent defects associated with FSW and its control strategies have been widely studied in order to expand the adoption of FSW in industrial areas (Meng et al., 2021, 2022).

2.4.1 FSW Process Parameters

The main FSW process parameters are tool rotational speed, traverse speed, and tool offset. Several experiments have been conducted to investigate the effect of FSW parameters on the weld appearance, the microstructure of the weld zone, the thermal and electrical properties, and, most importantly, the joint strength (Singh et al., 2019). In the case of dissimilar FSW, a suitable operating range of the process parameters must be carefully chosen to ensure adequate heat input is supplied, allowing appropriate material flow between the weld materials and hence, forming a quality joint.

2.4.2 Effects of Tool Rotational Speed

The rotational speed of the tool is a critical process parameter that has a significant impact on heat generation during dissimilar FSW. The turning motion of the tool around its axis generates frictional heat, which affects the plastic deformation of the weld materials. Adequate heat generation provides sufficient axial force, which influences the material flow, the size of the stir zone, and the IMC formation. When joining Mg to steel, the selection of tool rotational speed must be optimized. Low rotational speed would result in low heat generation, which causes inadequate intermixing of deformed materials throughout FSW of dissimilar Mg and steel. A study reported that the rotational speed of less than 900 rpm would lead to the formation of micro holes due to insufficient heat input and poor material filling (Singarapu et al., 2015). Similar defects were also reported in other dissimilar FSW when operated at low tool rotational speed (Abdollah-Zadeh et al., 2008; Bisadi et al., 2013; Esmaeili et al., 2011). Increasing the tool rotational speed would increase the heat generation during FSW, further softening the weld materials and promoting more reaction to take place between Mg and steel in the stir zone. However,

extremely high tool rotational speed causes excessive stirring of materials by the tool pin, fragmenting huge amount of metal particles from the base plate, making it hard for the fragmented particles to disperse homogenously in the stir zone (Singh et al., 2019). This causes inappropriate joining between the weld materials and attracts weld defects such as cracks and voids at the surrounding of fragmented metal particles (Bisadi et al., 2013; Schneider et al., 2011). In addition, higher heat generation as a result of faster rotational speed supports the formation of IMC at the interface. An increase in tool rotational speed produced thicker IMC layer (Kasai et al., 2015). A study on the relationship between thickness of IMC layer and joint tensile strength showed a relatively lower strength was obtained when thicker IMC layer was formed under high heat input condition (Kasai et al., 2015). Therefore, it is important to select optimal rotational speed when joining Mg and steel using FSW since both extremely low and high tool rotation degrade the joint qualities and its mechanical properties.

2.4.3 Effects of Traverse Speed

The speed at which the tool moves translationally along the joint line is referred to as traverse speed. It is also one of the critical FSW process parameters, which governs workpieces heating during the process. The amount of heat produced during FSW is proportional to the traverse speed. In other words, lower traverse speed generates more heat during the process as opposed to the higher tool traverse speed. Similar to tool rotational speed, traverse speed affects the heat generation during FSW which consequently impacts the mechanical properties of Mg-steel joint (Movahedi et al., 2012). When investigated the characterization of Mg-steel interface after FSW, the joint produced at traverse speed 150 mm/min detected a large amount of Fe in the Mg side due to the presence of steel particles in the region (Schneider et al., 2011). The high traverse motion of the tool resulted in insufficient heat generation in the stir zone, producing imperfect joint at the interface (Akinlabi et al., 2011). Low heat generation as a result of

high traverse speed also led to improper intermixing of dissimilar weld materials that generated defects such as voids and cracks (Akinlabi et al., 2011; Schneider et al., 2011). Reducing the traverse speed increases the FSW process temperature, which improves the materials flowability and reduces the defect formation (Kim et al., 2006). This is because sufficient process temperature obtained during low traverse speed carries more deformed material around the tool pin, which enhances the intermixing between the weld materials (Saeid et al., 2010). Therefore, when joining dissimilar materials, lesser traverse speed while keeping higher rotational speed are recommended for getting high quality joints (Singh et al., 2019).

2.4.4 Effects of Tool Offset

Tool offset refers to the position shift of the tool from the joint center line towards to the left or right side of the workpieces. The absolute zero position of the tool can be varied in different FSW setup, but in general, zero tool position is set as reference when the tool axis rotation is aligned perfectly with the joint center line. The location of tool pin that visualized its offset position is shown in Figure 2.10.

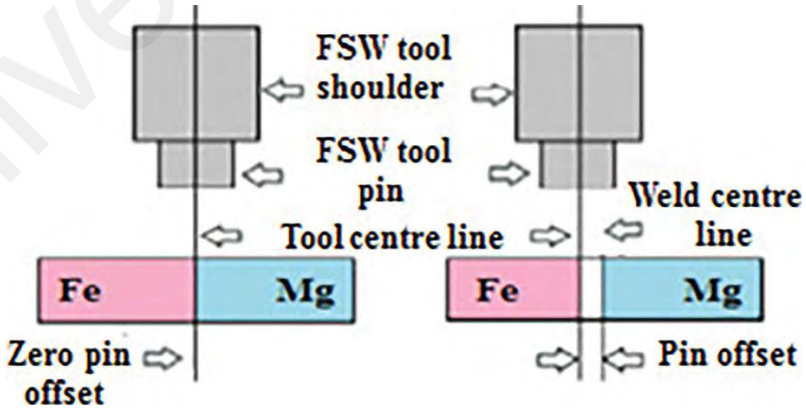

Figure 2.10: Schematic diagram of tool offset position (Singh et al., 2019)

Using a zero tool offset in dissimilar Mg-steel FSW produced defective and faulty joints due to many variances in thermal and mechanical properties of the materials (Kasai et al., 2015; Kumar et al., 2015). In addition, hard steel workpiece acts as an obstruction

towards material flow in the stir zone during the FSW process. Considering the mentioned concerns, offsetting the tool to Mg side is suggested as the hardness of Mg is lower than steel and the thermal conductivity of Mg is more as compared to steel, which produces extra heat over the Mg side and enables the heat to dissipate more properly (Singh et al., 2019). Past studies confirmed that positioning the tool pin towards the softer and lesser thermal conductivity material controls the development of fragmented particles in the stir zone that ensures sound and defect-free joints (Kasai et al., 2015; Lee & Jung, 2004; Ouyang et al., 2006; Shah & Tosunoglu, 2012). The optimal tool offset value is highly depending on material properties, workpiece thickness, tool geometry, other set of parameters (Hou et al., 2022). For FSW between Mg alloys and steel, a pin eccentricity of 1 to 2 mm was recommended to achieve the sound quality dissimilar joint (Kasai et al., 2015).

2.5 FSW of Magnesium Alloy and Steel

FSW between Mg and steel is difficult mainly because of the vast differences in the materials' mechanical and thermal properties. Because of these differences, the Mg-steel joint produces by FSW experiences immiscibility due to lacking IMC formation. The absence of essential IMC layers at the Mg-steel joint interface results in a poor metallurgical bonding between the weld materials, which greatly affects its mechanical properties (Kasai et al., 2015; Schneider et al., 2011). Therefore, the strength of Mg-steel joint can be improved with the presence of thin IMC layer at the joint interface.

Kasai et al. (2015) reported that successful Mg-steel joints were obtained when Mg alloys such as AZ31 and AZ61 were used to join with low carbon steel using FSW. The study showed that the increase in percentages of Al in Mg alloys improved mechanical properties of the joint. SEM images and EDS mappings of the cross-section interface as

shown in Figure 2.11 confirmed that the IMC layer consisting of Fe and Al elements was formed at the joint interface when the Mg specimens contained Al.

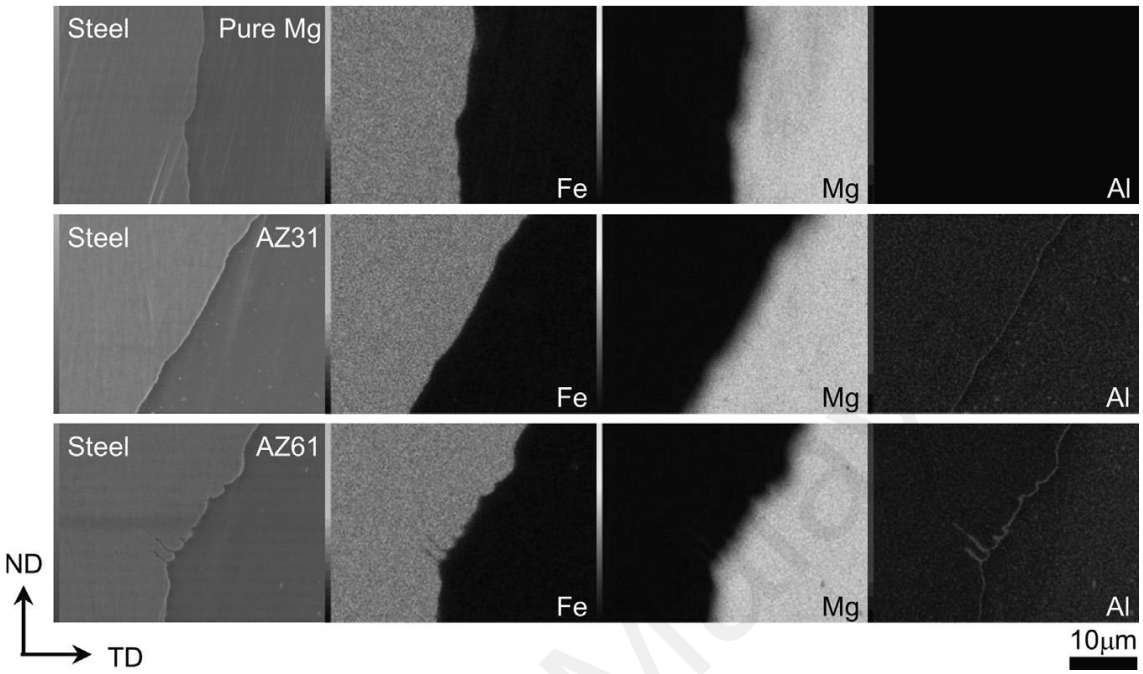

Figure 2.11: SEM images and EDS mappings of the Mg-steel interfaces (Kasai et al., 2015)

FSW between high Al content of Mg alloy also produced a joint with highest tensile strength, which was attributed by the development of Al-Fe IMC at the joint interface. Further observation on the fractured surface showed that the Mg-steel joint mainly fractured on the Mg side near the interface. The investigation implied that the IMC layer was stronger than the Mg side, thus determining the Mg-steel joint strength. Another study conducted by Chen & Nakata to assess the joinability of AZ31 alloy with brushed finish steel and zinc (Zn) coated steel revealed that a successful joint was obtained for AZ31 and Zn coated steel with a maximum failure load of up to 2.3kN whilst no joint was able to produce for AZ31 and brushed finish steel (Chen & Nakata, 2010). The presence of Zn coating assisted the development of Mg-Zn compound at the joint interface which improved the joinability of Mg alloy and steel. When investigating the effect of reactive alloy elements on FSWed Mg-steel joint, AZ31 and WE43 Mg alloys

were butt-joined with 316 stainless steel to identify the role of various intermetallic forming alloying elements on the strength of the dissimilar joints (T. Wang et al., 2019). Interdiffusion between the alloying elements in Mg alloys and steel was confirmed through TEM observations and EDS point analysis on the joint interface as shown in Figure 2.12.

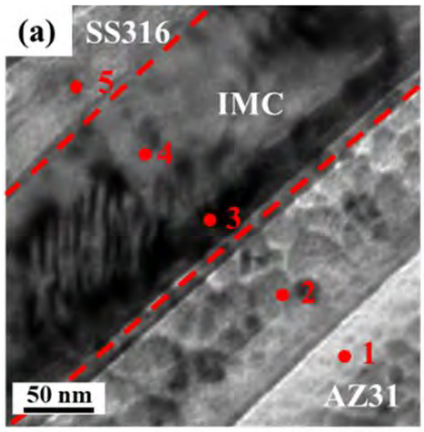

EDS point analysis results on each point in at. %

Element	Point 1	Point 2	Point 3	Point 4	Point 5
Al	2.77	-	28.5	28.16	-
Fe	29.22	10.86	15.16	37.98	51.49
Cr	9.0	3.28	4.82	11.22	22.06
Ni	2.8	1.44	2.50	5.08	6.51

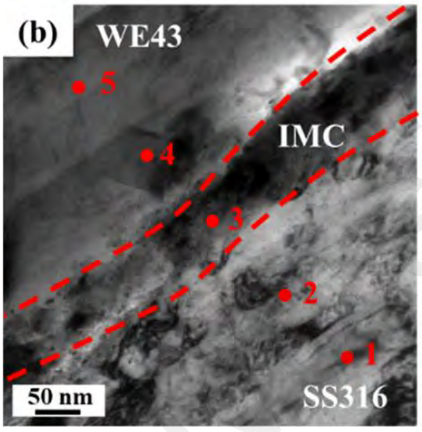

EDS point analysis results on each point in at. %

Element	Point 1	Point 2	Point 3	Point 4	Point 5
Y	-	2.12	1.68	0.31	0.32
Nd	-	7.52	0.25	1	1.09
Fe	54.03	52.44	41.25	0.6	-
Cr	23.4	16.27	20.98	-	-
Ni	5.32	2.05	-	0.96	-

Figure 2.12: TEM images and EDS point analysis on the interface of (a) AZ31-SS316 and (b) WE43-SS316 (T. Wang et al., 2019)

Alloying elements in Mg alloys diffused towards the interface to form Al-rich region in AZ31-SS316 and Y-Nd-rich region in WE43-SS316 joint interfaces. EDS point analysis showed that multiple IMCs such as $Al_{13}Fe_4$, ZnFe, $Fe_{17}Y_2$, and Fe_8Nd could form during FSW between Mg alloys and steel. The reported tensile strength of both dissimilar joints was 160 MPa, implying that there was no significant difference in the joint strength of FSWed AZ31-SS316 and WE43-SS316. The IMC thickness for AZ31-SS316 joint appeared to be thicker than that of WE43-SS316.

2.6 Friction Stir Alloying

The FSW method has been continuously expanded and much attention have been paid to overcome the immiscibility issues between dissimilar Mg and steel. It is well-established that a sound dissimilar joint can be achieved by promoting interfacial reactions between the weld materials and an innovative method to achieve that is by using filler materials as additives (Hou et al., 2021). In recent years, researchers have been adopting the use of thin interlayer and nanoparticles the reduce the immiscibility gap and obtain metallurgical bonding at the joint interface (bin Muhamad et al., 2021; Raja et al., 2022).

Friction stir alloying (FSA), which derives inspiration from FSW, has received growing attention as a surface modification technique and fabrication of metal-matrix composites (MMC) (Sharma et al., 2020). FSA is a reinforced FSW, in which the alloying materials are implied in the workpiece materials at the joining interface or at a defined area for localized property improvement (Karthik et al., 2017). In recent years, FSA has gained extensive interest as a composite joint formation technique by employing suitable additive at the interface of the welding materials. Research by Sun & Fujii (2011) demonstrated the effect of SiC particles on mechanical properties of Cu plate joints produced by FSA process. It was observed that the SiC dispersed Cu joints exhibited a much higher Vickers hardness as compared to the joints without SiC particles. Microstructural observation also confirmed that the SiC particles served as the heterogenous nucleation site in the dynamic recrystallization of Cu grain, therefore improving the hardness of the stir zone. In another experiment, Inada et al. (2010) employed the addition of dissimilar metal powder to fabricate alloyed joint between A1050-H24 plates. With the addition of Cu powder at the abutting edges of the plates, Al_2Cu precipitates were formed in the stir zone and consequently improved the hardness of the alloyed joint. Muhamad et al. (2020) conducted an experiment using Al-Ni powder

on FSA between Al alloy and 304 L stainless steel in the butt joint configuration. It was revealed that the joint tensile strength for specimen with Al-Ni powder enhanced remarkably than that of specimen without powder additive. This had been attributed to the significant mixing of Al-Ni powder with the base materials, which resulted in the increased joining strength. A similar technique was later performed by Muhamad et al. (2021), where they utilized the addition of Al-Mg metal powder on FSA between AZ31 alloy and mild steel as reinforcement additives for immiscible materials. The study reported that the addition of Al-Mg powder successfully enhanced the tensile strength of the joint by approximately 60% than the tensile strength of AZ31 and 38% than the tensile strength of steel. TEM images of Mg-steel interface as shown in Figure 2.13 revealed that a thin IMC layer, measured between 20-26 nm in thickness was detected after the processing. The IMC appeared to be consistently present along the joint interface with its thickness almost constant throughout the interface. The existence of Al-Mg powders supported the formation of Al-Fe IMC, which have led to the improvement in tensile strength of the joint.

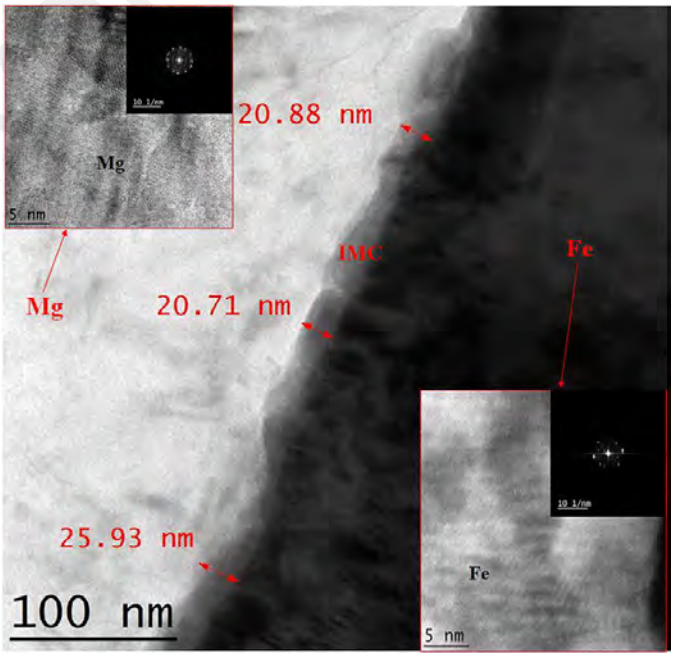

Figure 2.13: TEM image of the IMC at Mg-Fe joint interface with its corresponding FFT of base Mg and Fe (bin Muhamad et al., 2021)

2.7 IMC Formation in Dissimilar Magnesium and Steel Joining

The formation of intermetallic compounds is a significant consideration in dissimilar joining as it can contribute to both positive and negative effects on the joint. Many studies have been conducted with aims to examine the effects IMC formation on the joint strength however a consistent conclusion is yet to be reached. Mofid & Loryaei (2019) when investigating microstructural evolution at the interface of friction stir lap-welded (FSLW) of Al-Mg alloys reported that poor mechanical properties in the dissimilar joints of Al-Mg alloys were obtained because of the formation of $Al_{12}Mg_{17}$ and Al_3Mg_2. In contrast, Rao et al. (2015) reported that the strength of Mg-Al produced by friction stir spot welded was improved due to the interlocking of Al_3Mg_2 with dispersed $Al_{12}Mg_{17}$, which hindered the crack propagation thus improving joint mechanical properties. In another study, the author reported that the strength of friction stir welded of Mg and steel joint improved when more wt.% of Al powder reinforcement was added, which facilitated the formation of Al-Fe IMC at the interface (bin Muhamad et al., 2021). When joining steel to different types of Mg alloy via FSW, it was found that the strength of the joint increased when the Al content in Mg alloy increased, which promoted diffusion of Al into steel and thus forming an IMC layer (Kasai et al., 2015). The necessity of IMC was also studied by Kasai et al. (2015), which found that the increase in thickness of IMC led to deterioration of joint strength. The author revealed that an Al depletion region in Mg was developed as the Al in Mg was utilized for the creation of IMC. However, the IMC formed must be thin for preventing brittle fracture at the IMC. In addition to Fe-Al IMC, other IMC may also form during dissimilar FSW of Mg alloy and steel, which highly dependent on the alloying content, such as $MgZn_2$, Al_2Cu, and Cu_2Mg (Q. Wang et al., 2016; Zheng et al., 2019).

The creation of IMC in dissimilar joining have been identified with two formation mechanisms (Kostka et al., 2009). Firstly, IMC can form through the reaction between

molten weld materials when the welding temperature approaches or surpasses the temperature of the eutectic reaction. Secondly, IMCs can be generated through a diffusion reaction in the solid state. In the present study, IMC is expected to be generated through solid-state diffusion since the FSA peak temperature will not surpass the melting point of Mg alloy through parameter controls. A study conducted by P. Peng et al. on the IMC formation mechanism of friction stir lap welded (FSLW) of Mg and Al alloys reported that high probability of collision between Mg and Al atoms would result in the generation of Al12Mg17 phases (Peng et al., 2021). When studying the evolution mechanism of IMC during FSLW, it was reported that deformation induced by the stirring tool causes large numbers of Al and Mg atoms to collide, which resulted in the formation of the Al12Mg17 phase. It was also reported that further deformation gradually increased the IMC content as the collision between Mg and Al atoms were more. This is because the heat generation from friction and plastic deformation provided sufficient temperature for the diffusion reaction. Furthermore, the stir tool improved the rapid collision of atoms, which promoted the conversion of the kinetic energy of the atoms into thermal energy and then provided further heat for the diffusion reaction.

In summary, intermetallic compounds can offer unique properties and advantages in specific applications, but their formation, properties, and drawbacks depend on various factors. Researchers and engineers continue to explore ways to control and tailor the formation of intermetallic compounds in dissimilar FSW to achieve reliable and high-performance joints.

2.8 Nanomaterials Reinforcement in FSW and FSA

To strengthen Mg-steel joint, various FSW techniques have been attempted, which generally aims to overcome the immiscibility between these materials. One method to achieve a successful joint between immiscible materials is by introducing a filler material

as a reinforcement additive. Researchers have been utilizing nanoparticles and thin interlayer as additive to reduce the immiscibility gap and promote interfacial reaction between the welding materials (bin Muhamad et al., 2021; DQ et al., 2015; Raja et al., 2022). The introduction of filler materials as reinforcement additive in dissimilar materials joints have also received much attention. Friction Stir Alloying (FSA) which derives inspiration from FSW, can be utilized to produce composite joints using powder additive.

The usage of carbon nanotubes (CNTs) as reinforcement nanomaterials has gained extensive attention, especially in the fabrication of MMCs due to the potential use of CNT-reinforced MMCs in structural applications. Owing to its superior mechanical properties, CNT serves as an assuring reinforcement nanomaterial for strengthening the mechanical performances of MMC (Huang et al., 2018). Numerous research works (Esawi et al., 2010; M. Mishra et al., 2021; Sharma, Fujii, et al., 2020; Wei et al., 2021) have been conducted to incorporate CNT into metal matrix to enhance mechanical properties such as high tensile strength, high stiffness, and excellent elongation. In a study by Esawi et al. (2010) on the fabrication of Al-CNTs composite using powder metallurgy technique, they observed a significant improvement of up to 50% in tensile strength and 23 % in stiffness as compared to pure Al. Liang et al. (2017) when developing the CNT-reinforced Mg matrix composite via friction stir processing (FSP) and ultrasonic-assisted extrusion, revealed an enhanced mechanical strength of the composite due to dislocation strengthening and stress transfer mechanisms provided by CNT. A similar study by Du et al. (2016) also reported a significant improvement of yield strength and Vickers hardness of Al-CNT composite after the incorporation of CNT into the Al matrix using FSP.

2.9 Research Gap and Summary

Despite numerous studies on the impact of CNT on metal composites that have been conducted, research on the use and application of CNT as reinforcements in dissimilar joining is still limited. Furthermore, an approach to facilitate the construction of IMC at the joint interface of immiscible materials is worth exploring to achieve better joint properties from a metallurgical standpoint. Therefore, the present research aims to investigate the effects of Cu-CNT powder additives on the microstructural evolution and mechanical behavior of AZ61 Mg alloy and mild steel composite joint produced by FSA technique. Cu powder was selected as a filler material for the following reasons:

1. Cu could react with Mg to form two intermetallic phases which are Mg2Cu and MgCu2 and form solid solution with Fe. Remaining Cu particles that unable to dissolve in Fe provides chances for the element to interact with Mg element, therefore giving rise to the formation of Mg-Cu IMCs. The construction of Mg-Cu IMCs was expected to serve as a strengthening mechanism for Mg-steel joint by enabling metallurgical bonding at the interface.

2. Cu element would lower the reaction temperature between Mg, Fe, and Al elements. This would broaden the temperature range of solid/liquid transformation and the metallurgical reaction between these elements. Since this is a solid-state joining technique, its process temperature is relatively lower than the melting point of Cu. Thus, the reaction between Cu and Mg elements was made possible through solid-solid diffusion by means of severe plastic deformation.

3. Cu plays a role in promoting diffusion process at the interface which improves the inter-diffusion of Mg, Al, and Fe. Thus, Cu powder-added joints was expected to demonstrate higher tensile strength as demonstrated in tensile test results.

On the other hand, the use of CNT as reinforcement nanomaterials is expected to provide an additional reinforcement for the joint through various strengthening mechanisms, therefore improving the joinability and mechanical properties of Mg-steel joint. Thus, FSA technique is employed in this experiment to achieve both IMC formation and nanomaterials interaction during the immiscible joining process.

CHAPTER 3: MATERIALS AND METHODOLOGIES

In Chapter 3, the methodologies employed to conduct FSA experiment and analysis to meet the research objectives are explained. This chapter outlines the types of materials and tools used for the experiment, methods of the FSA experimentation, and the analysis involved. Figure below illustrates the flowchart of the research.

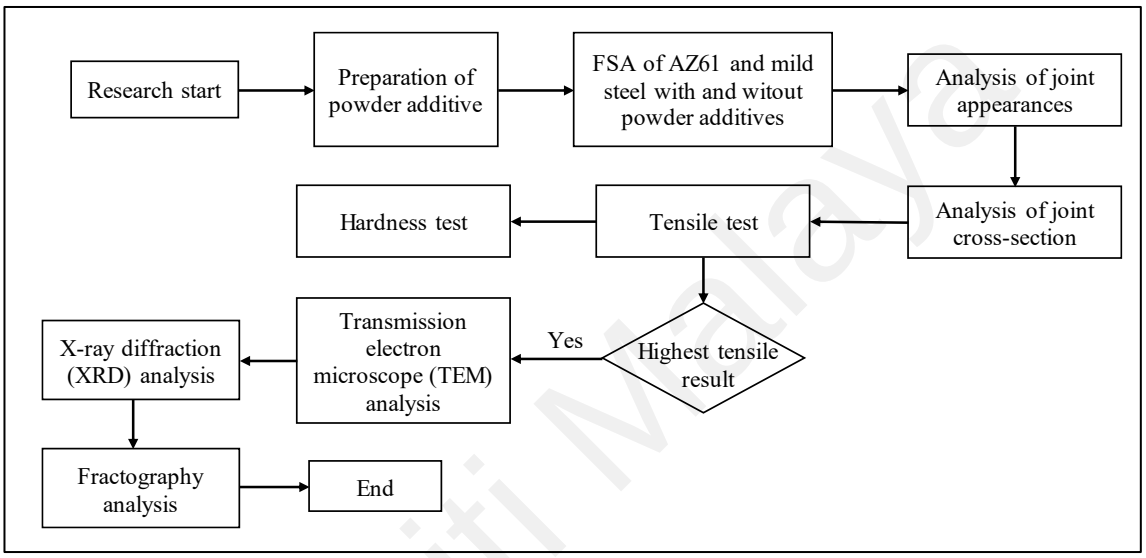

Figure 3.1: Flowchart of experimentation

In the following section, details of materials, powder additives preparation, FSA methods, and analysis conducted were explained.

3.1 Materials

3.1.1 Base Materials

Steel Plate Hot-Roll Coiled (SPHC) mild steel (Fe-0.12 wt.% C-0.60 wt.% Mn) and AZ61 (Mg-5.85 wt.% Al-0.65 wt.% Zn) magnesium alloy plates with dimensions of 50 x 150 x 1.5 mm were used as the base materials in the experiment. The mechanical and thermal properties of the materials are shown in Table 2.

Table 2: Mechanical and thermal properties of the workpieces

Materials	Tensile strength (MPa)	Elongation (%)	Hardness (HV)	Melting Temperature (°C)
AZ61	265	16	68	650
Mild Steel	355	33	112	1480

3.1.2 FSA Tool

The tool used for the experiment was a cylindrical tool made of tungsten carbide, which dimensions were 12 mm in diameter and 30 mm in length. The cylindrical tool consists of a probe with a height of 1.3 mm and a diameter of 4 mm. The hardness of the tool is 65 HRC. The cylindrical tool was fabricated using a grinding machine with diamond wheel located in the student's workshop building. The schematic diagram of the tool together with its dimensions were illustrated in Figure 3.2.

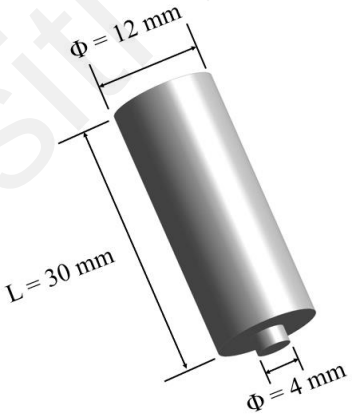

Figure 3.2: Schematic diagram of the FSA tool

3.1.3 Powder Additive Materials

The powder additive materials used in the experiment were Cu and CNT powder, which served as reinforcement materials for the FSA of Mg alloy and mild steel. In addition, polyethylene glycol (PEG) was used during the preparation of Cu-CNT additive solution. The purpose of using PEG during the preparation of additive solution was to prepare the Cu-CNT powder in the form of semi-solid. This was achieved by melting the

PEG before mixing with Cu-CNT powder to form a semi-solid paste. The semi-solid additive allowed smooth injection of Cu-CNT additive between the workpieces prior to FSA process. The semi-solid additive also helped keep the Cu-CNT powder in between the gap, preventing scattering of powders during the FSA process.

Copper powder (99.9% purity) used in this experiment was procured from ACROS Organic. The average particle size was 45 μm.

Multiwalled carbon nanotubes (MWCNT) (98% purity) was procured from Nanostructured & Amorphous Materials. The outer diameter of the MWCNT was ranging 30 nm to 80 nm, and the inside diameter was in the range of 5 nm to 15 nm. The average length of MWCNT was 10 μm.

Polyethylene glycol (PEG) was procured from Sigma-Aldrich and was used during the preparation of the additive. The molecular weight of PEG used in the current study is 2000, and its melting point is 50 - 53 ºC. As mentioned, PEG acted as a binding agent that adhered Cu and CNT powders together to form a semi-solid additive which aimed to avoid the scattering of powders during the FSA. This semi-solid additive also helped smooth the injection of additive in the FSA process. At elevated temperature during the process beyond 250 ºC, PEG decomposed and evaporated with no traces remain.

3.2 Preparation of Additive Solution

Cu powder with 1, 3, and 5 wt.% of CNT was prepared using ultrasonication and magnetic stirring. Firstly, 1 wt.% of CNT was placed into the beaker containing 10 ml of ethanol. The mixture was then subjected for ultrasonication for 20 minutes to ensure proper dispersion of CNT in the ethanol. Next, 5 g of Cu powder was added into the solution. The Cu-CNT solution was then ultrasonicated for 20 minutes for appropriate

mixing of Cu and CNT. After that, the Cu-CNT solution was stirred using magnetic stirrer for 1 hour to increase the homogeneity of Cu and CNT in the solution.

Before adding PEG into the Cu-CNT solution, 0.2 g of PEG powder was first added to a beaker containing 10 ml of distilled water and proceeded to magnetic stirring at 80 ºC for 1 hour to form a PEG solution. After that, the magnetic stirred Cu-CNT solution was added gradually into the PEG solution. Lastly the Cu-CNT mixture inside the PEG solution was subjected for another round of magnetic stirring for 30 minutes at 80 ºC. Similar methods were then repeated to prepare additives of Cu powder with 3 and 5 wt.% of CNT. The illustrative image of Cu-CNT additive is shown in Figure 3.3. All the facilities and equipment used in the preparation of Cu-CNT additives were provided in the Surface Engineering Lab of Mechanical Engineering Department.

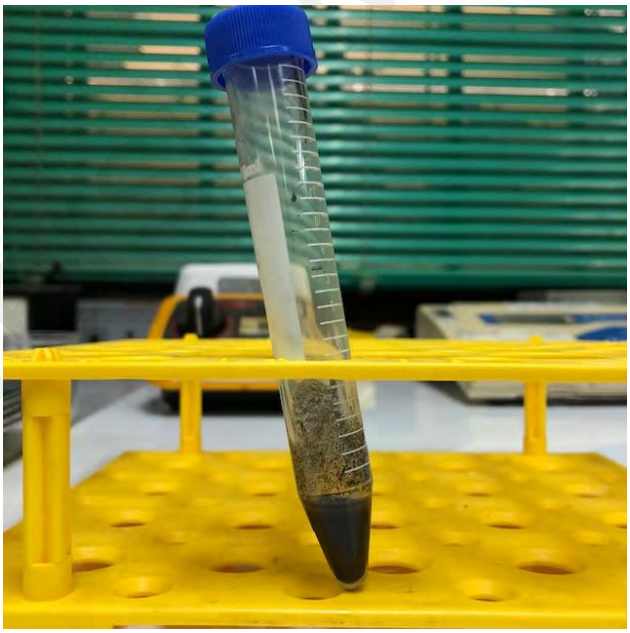

Figure 3.3: Cu-CNT additive prepared by ultrasonication and magnetic stirring

3.3 FSA Experiment between Mg and Steel with Cu-CNT additive.

The experiment was carried out using the modified Mitsui Seiki VT3A CNC Milling machine located in High-Speed Machining Lab with customized jigs and a pneumatic clamping system. For materials arrangement, AZ61 was placed on the retreating side and

SPHC mild steel was on the advancing side. The schematic of the FSA experimental setup and the actual experimental setup is shown in Figure 3.4(a) and Figure 3.4(b) respectively.

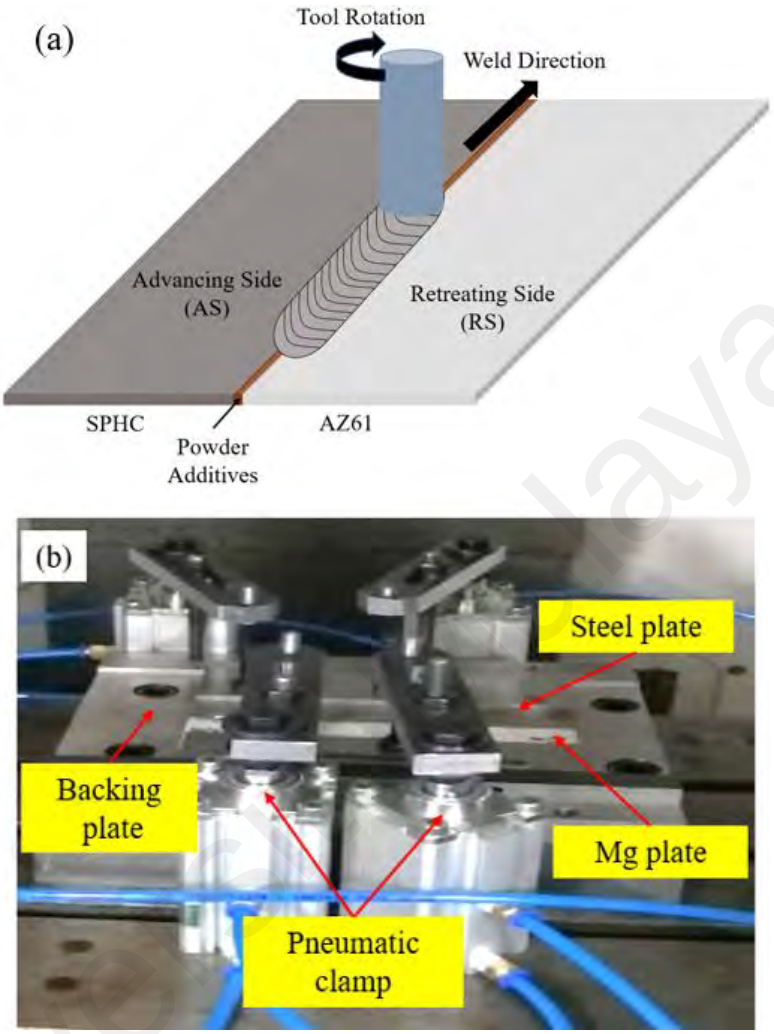

Figure 3.4: (a) Schematic diagram of FSA experimental setup and (b) actual FSA experimental setup

The tool shoulder was plunged 0.1 mm into the plates and the probe was offset by 1 mm into the butt side of SPHC. A zero offset is defined such that the probe is plunged into the AZ61 plate, and its side just touches SPHC's butt side surface. The setup was achieved by calibrating the rotating head with FSA tool attached until the probe's side contacted the steel's butt side surface, before setting the offset reference as "0 mm". Therefore, a positive offset is obtained as the position of the probe shifts horizontally across the width of the SPHC plate. The schematic diagram, which illustrated the tool

plunge depth and its offset positions are shown in Figure 3.5(a) and Figure 3.5(b) respectively.

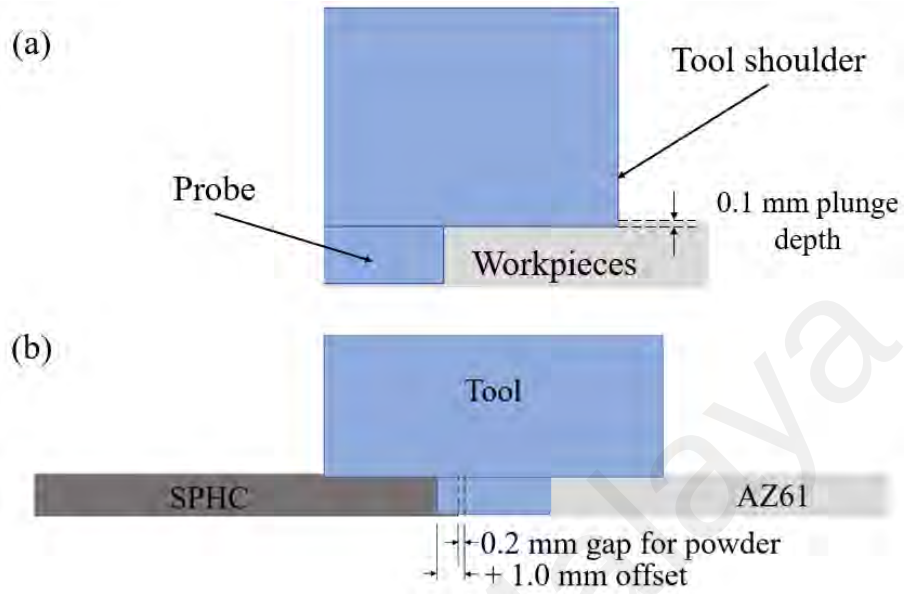

Figure 3.5: Illustration of FSA tool positioning (a) tool plunge depth and (b) tool offset positions

As discussed in section **Error! Reference source not found.**, the probe was brought o ffset towards the Mg side was due to the harder properties of steel as compared to Mg alloy, which acts as an obstruction towards material flow in the stir zone during the FSW process. Considering the mentioned concerns, offsetting the tool to Mg side was selected as the hardness of Mg is lower than steel and the thermal conductivity of Mg is more as compared to steel, which produces extra heat over the Mg side and enables the heat to dissipate more properly.

The experiment was first conducted by producing FSW joints between Mg alloy and steel with no additive condition, then proceeded with producing FSA joints with only Cu additive, followed by Cu-CNT additive. For producing FSA joints with additives, Cu additive and Cu-CNT additive was first injected by using a syringe into the 0.2 mm gap between AZ61 and SPHC workpieces prior to the experiment. To ensure the additive filled up the gap entirely, the additive was injected till it overflowed from the gap and the

excess additive was scrapped off the workpieces using a metal plate. Mg-steel joints without additive and the joints with Cu and Cu-CNT additives were produced at varied traverse speeds between 15 mm/min and 50 mm/min, and at a constant rotational speed of 1500 rpm. In this experiment, the gap for additive was chosen to be 0.2 mm as it was the ideal gap to enable the additive to be filled in effectively between the Mg alloy and steel. Reducing the gap smaller than 0.2 mm made it hard for the additive to effectively fill the gap due to its semi-solid form. In addition, increasing the gap wider than 0.2 mm resulted in defective weld due to lesser volume of material was stirred in the stir zone. The parameter selections for traverse speed and tool rotational speed in this study were employed from research conducted by Raja et al., 2022, which utilized similar weld materials as this study. Aligning the parameter selection with published research that utilizes similar materials is expected to strengthen the reliability and the relevance of the findings of this study. Details of the FSA experiments, which showed variations of traverse speed and weight percent (wt.%) of CNT with respect to Cu powder were summarized in **Error! Reference source not found.**.

Table 3: Details of FSA experimental condition

FSA condition	Value
Tool rotation (rpm)	1500
Tool offset (mm)	1.0
Probe length (mm)	1.3
Probe intrusion depth (mm)	1.4
Traverse speed (mm/min)	15, 30, 50
Material thickness (mm)	1.5
Additive condition and percentage (wt.%)	Without additive, only Cu, Cu with CNT 1, 3 and 5 %
Copper powder average diameter (μm)	45
Diameter of CNT dimension (nm)	50-80

3.4 Mechanical Properties Analysis

The mechanical properties of the Cu-CNT added Mg-Fe joints were analyzed based on tensile and microhardness tests.

The tensile specimens as shown in the schematic diagram in Figure 3.6 were prepared in accordance with ASTM: E8 sub size standard using a wire Electrical Discharge Machining (EDM) machine.

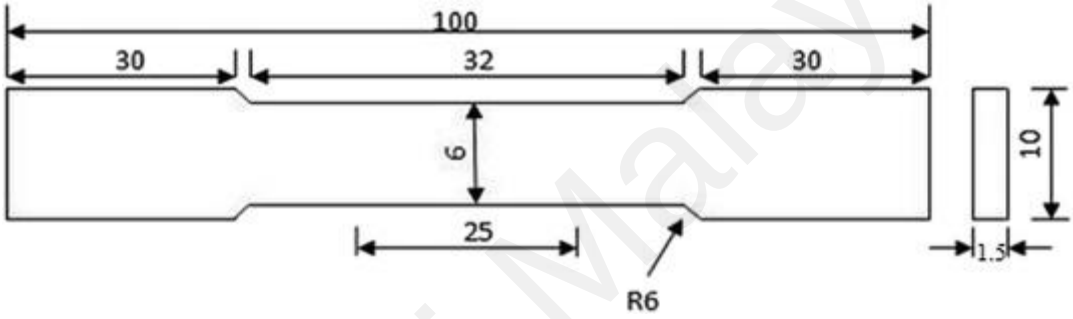

Figure 3.6: ASTM E:8 tensile test specimen (dimensions are in mm)

Tensile analysis of the prepared specimen was conducted using a Universal Testing Machine (INSTRON Model 3369) in Fundamental of Materials Lab, at a constant loading rate of 0.5 mm/min perpendicular to the joint line. As such, the strain rate, ϵ for the tensile test can be calculated as equation (3.4.1), in which $v(t)$ is the loading rate and L_0 is the initial specimen length.

$$\epsilon = \frac{v(t)}{L_0} \tag{3.4.1}$$

$$\epsilon = \frac{\frac{0.5\ mm/min}{60^{-s}}}{100\ mm} = 8.33\ X\ 10^{-5} s^{-1}$$

Three specimens were tested for each FSA joint and the average results for each condition were calculated. Figures of the tensile test equipment and ASTM: E8 standard tensile specimens are shown in Figure 3.7(a) and Figure 3.7(b) respectively.

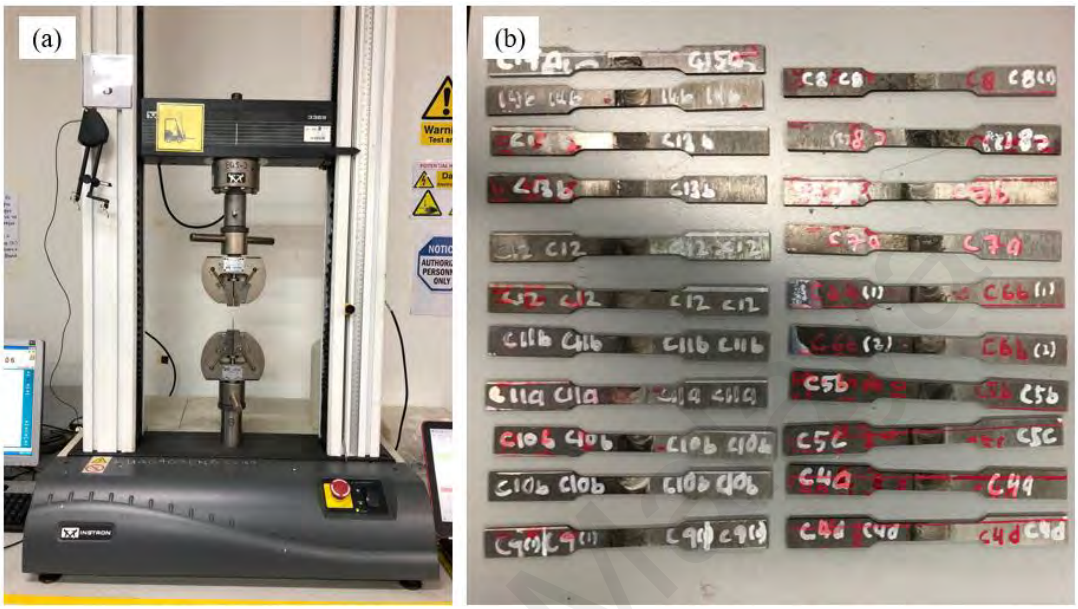

Figure 3.7: (a) INSTRON 3369 universal testing machine and (b) ASTM: E8 standard tensile test specimens

HMV 2T E Vickers microhardness tester provided in the Surface Engineering Lab, as shown in Figure 3.8, was used to measure the hardness along the cross-sectional region of the interface.

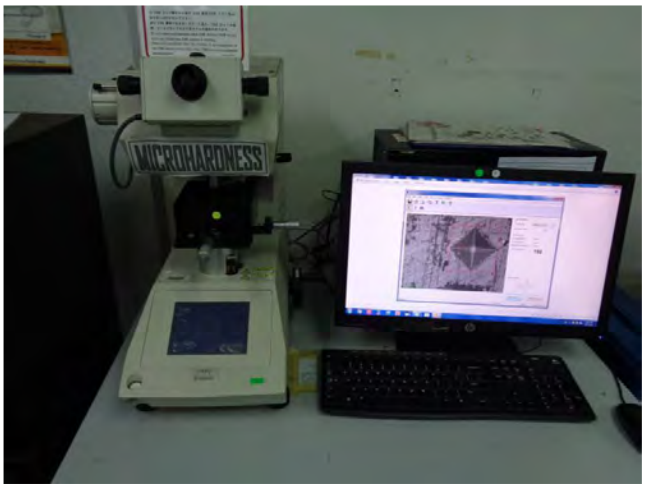

Figure 3.8: HMV 2T E Vikcers microhardnesss tester

Hardness values were measured at 0.75 mm from the top surface for every 0.5 mm along the cross section of the joining region as shown in Figure 3.9, at which the center of the stir zone was defined as the zero position, and positive distance is obtained when the point moves further from the joining center line towards the steel side.

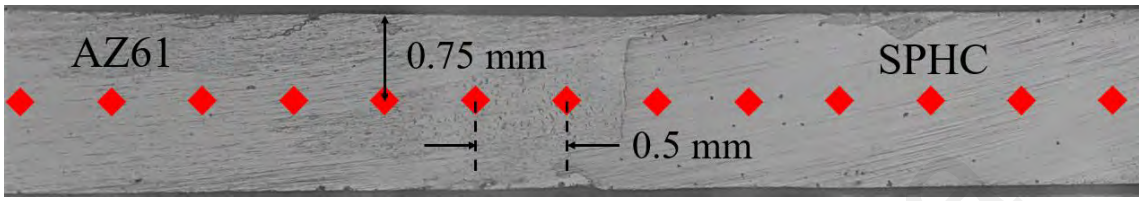

Figure 3.9: Location of hardness measurement along the joint cross-section

The analysis was performed using a diamond pyramidal indenter with the idented load of 980.7 mN for a dwell time of 5 seconds.

3.5 Microstructural Analysis

Microstructural analysis in the present experiment were conducted for observations using optical microscope (OM, Olympus BX61), x-ray diffraction (XRD, Panalytical Empyrean), a field emission-scanning electron microscope (FE-SEM, Quanta FEG 450), and a transmission electron microscope (TEM, FEI Tecnai G2 F20).

For OM observations, the joints were cross-sectioned and progressively polished using increasing grades of emery paper up to 5000 grits followed by 1 µm diamond suspension. The macroscopic images of the joint cross-sections were observed using Olympus BX61 microscope.

For TEM observations, a thin lamella with about 18 µm length and 100 nm thickness was extracted from the Mg-steel joint interface using FEI Helios Nanolab 650 focused ion beam (FIB) equipment. To prepare the lamella, the Mg-steel interface as shown in Figure 3.10(a) was sliced and trenched around the interface with ion beam bombardment as shown in Figure 3.10Figure 3.10(b) to extract the lamella from the specimen. Next, a

needle was used to pick up the lamella from the trench using platinum welding technique. Finally, the lamella was attached on a Cu grid and welded to the grid using platinum deposition method.

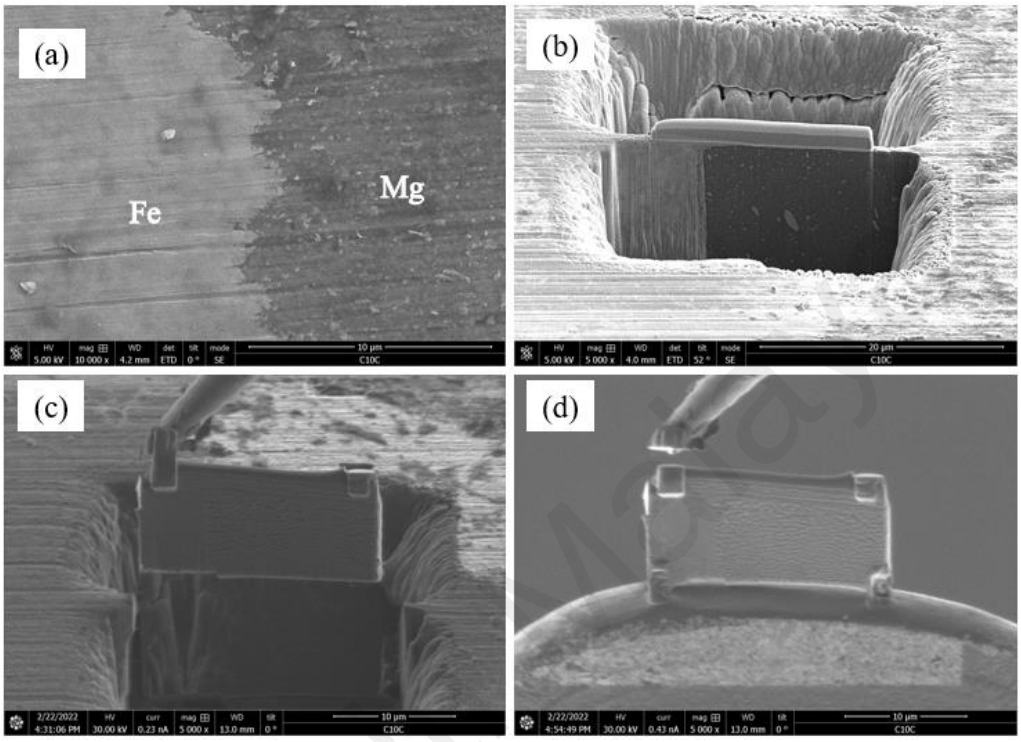

Figure 3.10: Lamella preparation using FIB from Mg-Fe joint interface (a) Mg-Fe interface, (b) trench digging around the lamella, (c) picking up of the lamella, and (d) mounting of lamella on Cu grid

Once the lamella was prepared, TEM images of the lamella were captured using FEI Tecnai G2 F20 TEM machine as shown in Figure 3.11 to identify the role of powder additive in facilitating the construction of IMC and their interfacial bonding within the interface. The imaging was conducted at 300 kV accelerating voltage. The preparation of lamella and TEM imaging was conducted at a research facility in the Malaysian Institute of Microelectronic Systems (MIMOS) Berhad.

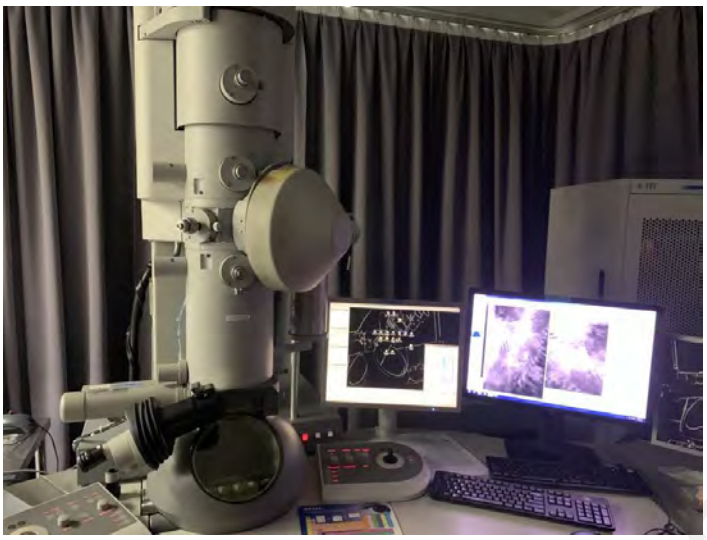

Figure 3.11: FEI Tecnai G2 F20 TEM Machine

For IMC phase analysis, XRD was conducted for the joint specimen using Panalytical Empyrean XRD equipment in the Central Advance Research Enabler Facility (CAREF) as shown in Figure 3.12. The analysis was conducted at diffraction angles of between 25 and 90°. The resulting data was processed using Xpert Highscore Software and matched with JCPDS ICDD database.

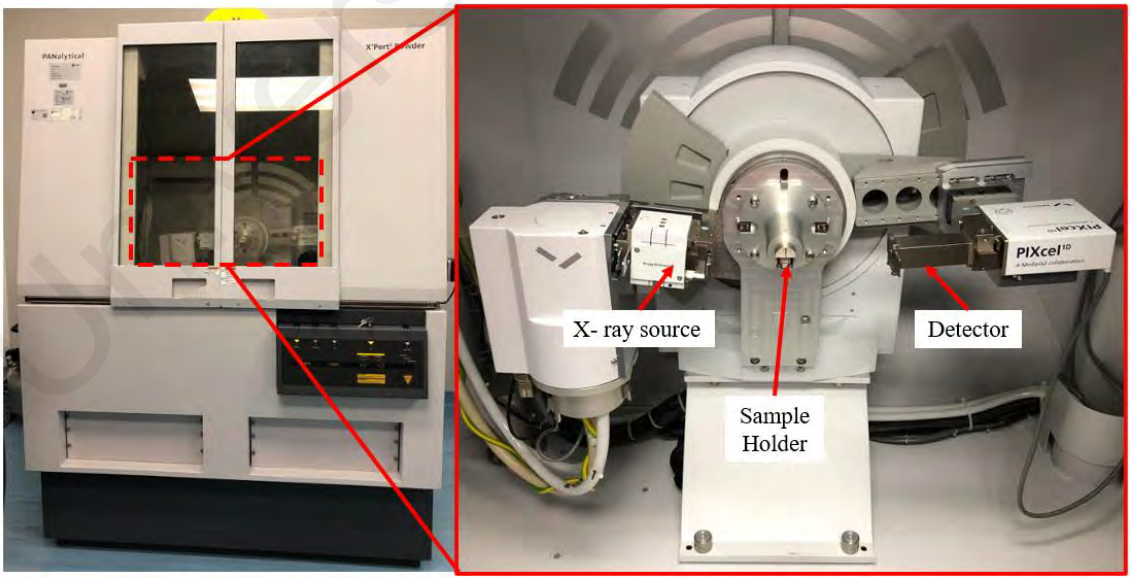

Figure 3.12: Panalytical Empyrean XRD Machine

Fractography analysis of tensile specimens was carried out via FE-SEM on model Quanta FEG 450 as shown in Figure 3.13 to identify the failure modes of the joint.

Figure 3.13: Quanta FEG 450 FE-SEM Machine

CHAPTER 4: RESULTS AND DISCUSSIONS

Chapter 4 presents the outcomes of FSA experimentation applied to magnesium (Mg) alloy and steel joints and the mechanical and microstructural analysis conducted. Within this topic, details of joint appearances, cross-sections at the joint interface, effect of Cu-CNT additive on tensile strength, microstructural characteristics of Mg-steel interface, role of Cu powder on the IMC formation, and the strengthening mechanisms involved were explained. This chapter first begins with discussions on the effect of different traverse speeds on Mg-steel joint appearances and joint cross-section. After that, a substantial portion of this chapter discusses on the effect of Cu-CNT additive on the joint tensile strength and the characteristics of Mg-steel interface in order to understand the strengthening mechanisms that attributes to the improved properties. Then, the chapter extends to discussion on the role of Cu powder on promoting metallurgical bonding between the dissimilar materials, FE-SEM observations of the fractured specimen and microhardness assessment to evaluate the effect of Cu-CNT powder additives on mechanical properties of the joints produce by FSA.

4.1 Joint Appearances

FSA between AZ61 and SPHC was carried out and the influence of different traverse speed on macro morphology of the joints was investigated. From Figure 4.1(a-j), it was observed that the joints produced at 15 and 30 mm/min resulted in good surface appearances without distinguished defects. However, observation on Figure 4.1(b) showed the appearance of burn marks just outside the joint seam, which was caused by the excessive heat input due to low traverse speed. On the other hand, FSA of AZ61 and SPHC produced at 50 mm/min resulted in surface lack of fill partly at the faying interfaces of the workpieces, as shown in Figure 4.1(m-n).

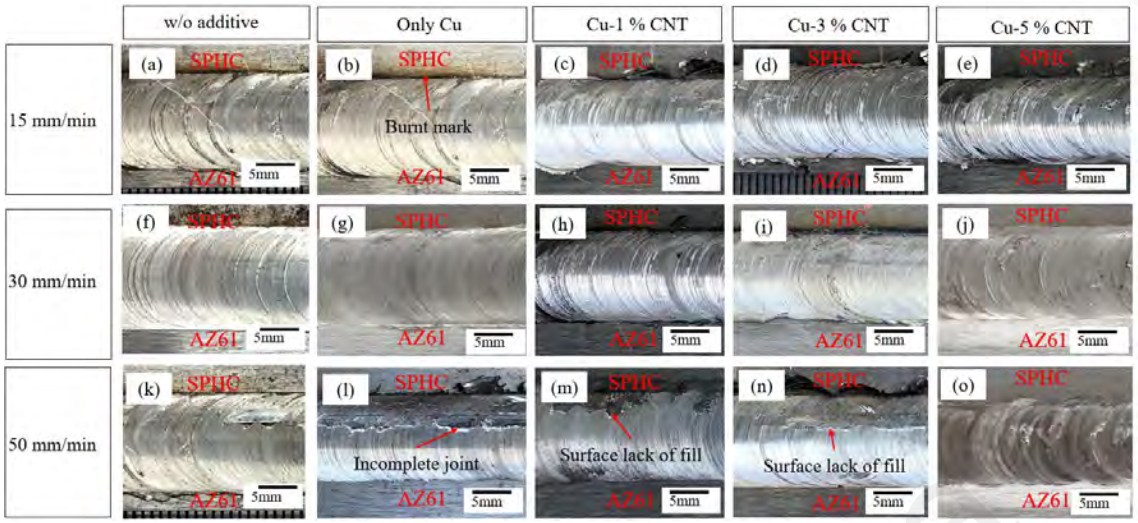

Figure 4.1: Joint appearance of FSA between AZ61 and SPHC at traverse speed (a-e) 15 mm/min, (f-j) 30 mm/min, and (k-o) 50 mm/min

The appearance of this defect was due to the increase in traverse speed, which resulted in a significant reduction of heat generation to the stir zone. As a result, the materials were not plasticized sufficiently. This caused higher flow stress that led to improper material movement around the tool and therefore hindered the materials consolidation (Khan et al., 2015). With the right combination of rotational rate and traverse speed, the heat generation by the tool is optimum, providing adequate heat input to the stir zone to plastically deform the materials and thus forming the joint. Based on the visual evaluation of joint appearances produced at three different traverse speed, all the Mg-steel joints produced at traverse speed of 30 mm/min resulted in the most consistent joint quality without distinguished defects as compared to the joint quality produced at 15 and 50 mm/min. As such, the parameter combination in which the FSA results were optimum was when the joints were produced at traverse speed of 30 mm/min and tool rotational speed of 1500 rpm.

4.2 Macroscopic Observations at Joint Interface

Figure 4.2 shows optical microscopic images of the cross section of Mg-steel joints with no powder-added produced at different traverse speed conditions. At traverse

speed 15, 30, and 50 mm/min, bent steel structures extended into the Mg side were observed near the bottom region of the joint interface. The formation of such structures at joint interfaces was due to the deformation by the tool, which illustrated the penetration of the probe into the workpieces. Macroscopic observation for joint specimen at traverse speed 15 mm/min as presented in Figure 4.2(a) shows random scattering of steel fragments in the Mg side in the stir zone. This is because FSW at low traverse speed generates greater stirring effect and forging of materials by the tool, which results in more steel particles to be fragmented from the base plate and subsequently dispersed into the stir zone (Singh et al., 2019). Increasing the traverse speed to 30 mm/min improved the flowability of the materials, resulting in a defect-less joint interface as shown in Figure 4.2(b). However, further increases of the traverse speed creates complexity in flowability of the materials due to inadequate heat generation as depicted in Figure 4.2(c). This reduced the stress flow during FSW which caused large steel fragments to be broken down from the base metal and inappropriately stirred into the Mg zone.

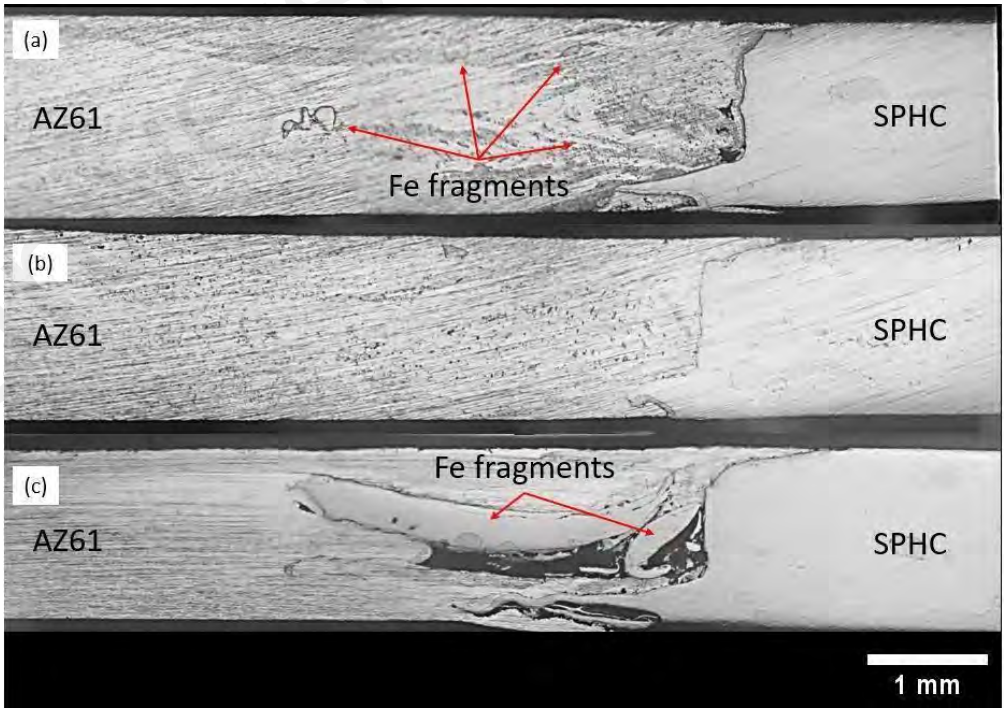

Figure 4.2: Macroscopic images of joint cross section at interface at traverse speed (a) 15 mm/min, (b) 30 mm/min, (c) 50 mm/min

4.3 Effect of Traverse Speed and Cu-CNT Additive on Tensile Strength

Figure 4.3 shows the effect of traverse speed and varied Cu-CNT compositions additive on tensile strength of the Mg-steel joint specimens.

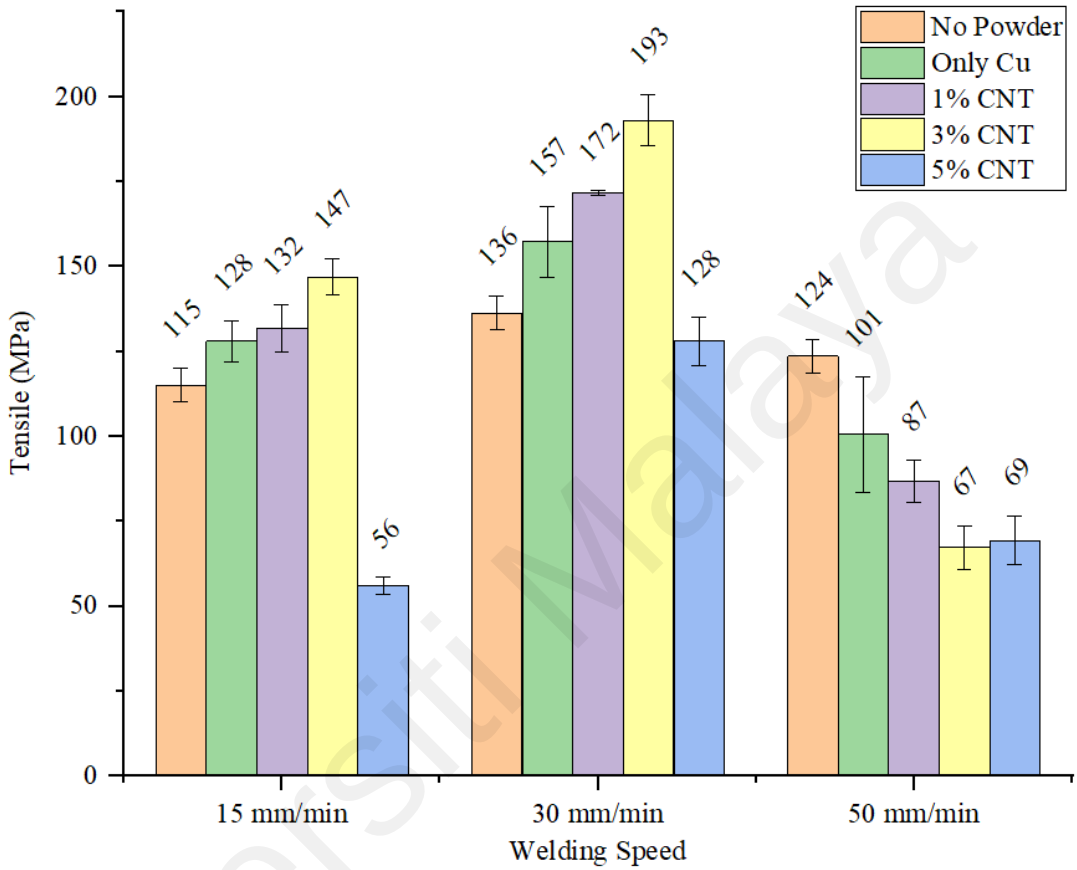

Figure 4.3 Joint tensile strength at different traverse speeds and additive compositions

The result shows that the tensile strength increased with increasing traverse speed from 15 mm/min to 30 mm/min. However, the tensile strength reduced when the traverse speed was further increased to 50 mm/min. The reason for this behavior was because high traverse speed reduced heat generation during the FSA and caused inappropriate intermixing of the dissimilar materials. Macroscopic observations of joint cross section performed at 50 mm/min, which can be seen in Figure 4.2(c) showed coarse fragments of steel disorderly dispersed in the stir zone as a result of inadequate flow of deformed materials. In dissimilar joining, non-uniform dispersion of metal particles, especially

coarse particles in the stir zone reduces the joint strength, as it can result in the formation of microcracks and voids around the particles (Saeid et al., 2010). Moreover, the substantial amount of fragmented steel particles existing near the joint interface indicates a complexity in flowability, which leads to poor joint formation between the dissimilar materials (Schneider et al., 2011). It is also worth noting that the FSW of Mg to steel without additive successfully formed a joint with considerable joint strength. Although there were lesser elemental interactions as compared to the ones with additives, the joining mechanism could be attributed to the mechanical interlocking at joint interfaces. As observed in Figure 4.2, all joint interfaces were bent with steel structures going into the Mg side. Such interlocking would promote a joint between the materials. Similar mechanism has also been reported in other studies, which suggested that such mechanical interlocking would play a role in promoting a joint of dissimilar welds (bin Muhamad et al., 2021; Kasai et al., 2015). In addition, the joining mechanism for Mg-steel without additive was the interaction of alloying elements in AZ61 with Fe, which could induce the formation of IMC. Although Mg and steel are metallurgically immiscible, IMC could be formed at the joint interface due to the existence of alloying elements in both magnesium alloys and steel (T. Wang et al., 2019).

On the effect of Cu-CNT additives, it was revealed that the joint tensile strength for specimens with powder additives were higher than that without powder additives at 15 mm/min and 30 mm/min. It was also revealed that the incorporation of CNT with Cu powder enhanced the joint tensile strength as compared to specimens with only Cu powder addition. However, incorporation of powder additives at traverse speed 50 mm/min caused a decrease in tensile strength. This could be due to the improper stirring of powder additives at high traverse speed, which hampered uniform dispersion of the powders inside the stir zone. It is noted that the joint tensile strength increased with the increasing volume percentage of CNT up to 3%, whereby any further addition of CNT

lessened the tensile values. The highest tensile strength of 193 MPa was achieved for specimen with Cu-3 % CNT produced at traverse speed of 30 mm/min, which gives the joint efficiency of 72 % with respect to the strength of base metals AZ61. The stress-stain curves of the base materials and the Mg-steel joint with the highest tensile strength is presented in Figure 4.4.

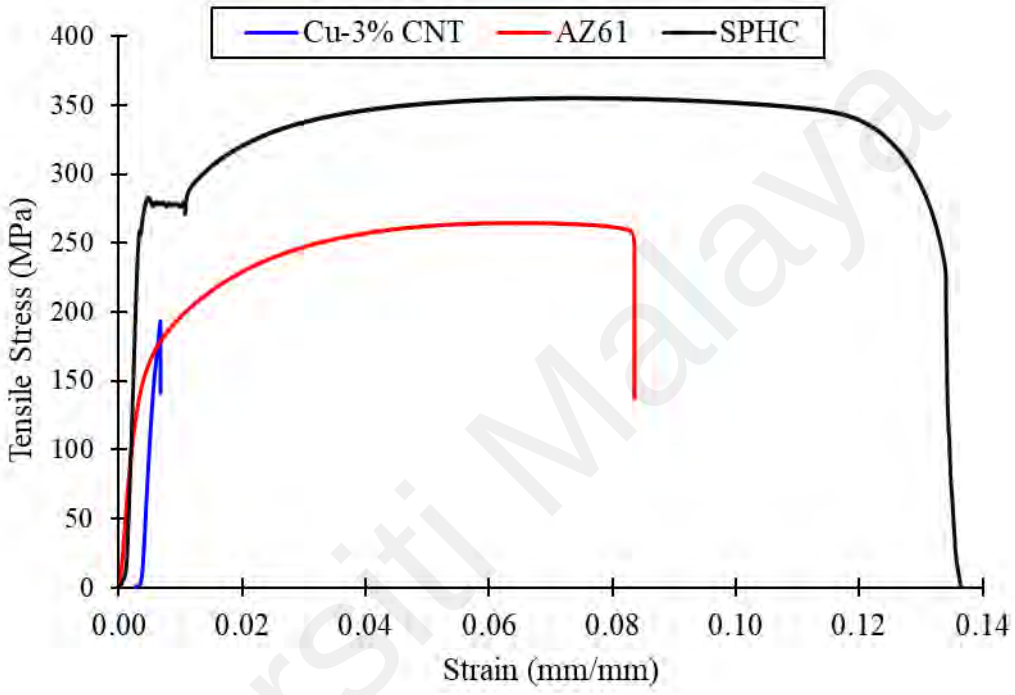

Figure 4.4: Stress-strain curves obtained by tensile test for AZ61, mild steel, and Mg-steel FSA with Cu-3 % CNT at traverse speed 30 mm/min

At the same traverse speed condition, the tensile strength for specimens without powder additives and only Cu additives were 136 MPa and 157 MPa respectively. Previous study conducted by T. Wang et al. (2019) on the effect of reactive alloying elements on the strength of butt-welded Mg alloy and steel reported a maximum tensile strength of 160 MPa. The authors mentioned an interdiffusion of alloying elements in Mg alloy into the welded interface region and steel matrix was occurred and the diffusion of these elements had led to the formation of IMC at the interface. In another study, Muhamad et al. (2021) produced dissimilar joint between AZ31 Mg alloy and mild steel with the help of Al-Mg powder additives. The tensile test results showed that the powder-

added joint demonstrated a significant enhancement of tensile strength of 150 MPa as compared to the strength of 125 MPa obtained for the joint with no powder additives. Further analysis on its microstructural features revealed that the powder additive was uniformly dispersed in the stir zone and the IMC layer was detected at the joint interface. Besides, they reported that the addition of Al-Mg powders compensated for the loss of alloying element in Mg alloy which helped construct the IMC layer, improving the joint tensile strength significantly. In this study, tensile test results showed that the addition of Cu-3 % CNT improved the joint efficiency of AZ61 and SPHC steel up to 74% with respect to base AZ61 as compared to only 52% for direct Mg-steel joint with no additives and 60 % for only Cu additives. However, a greater percentage of CNT addition resulted in notable reduction in tensile strength values. The reduction in strength could be attributed to the presence of agglomerated CNT in the stir zone, which impaired the joint mechanical properties (Liang et al., 2017; Srinivasan et al., 2021; Wei et al., 2021). At this point of analysis, it was presumed that the improved joint strength was attributed to the formation of IMC and strengthening mechanism by CNT. To confirm the effect of Cu-CNT powder additives on tensile strength, TEM analysis was performed for the joint specimen with the highest tensile result, which was Cu-3% CNT produced at traverse speed of 30 mm/min and discussed in the following section.

4.4 Characteristics of Mg-steel Interface by TEM Analysis

For TEM investigation, a thin lamella as shown in Figure 4.5, was obtained from Mg-steel joint interface produced at traverse speed of 30 mm/min with Cu-3%CNT powder additives.

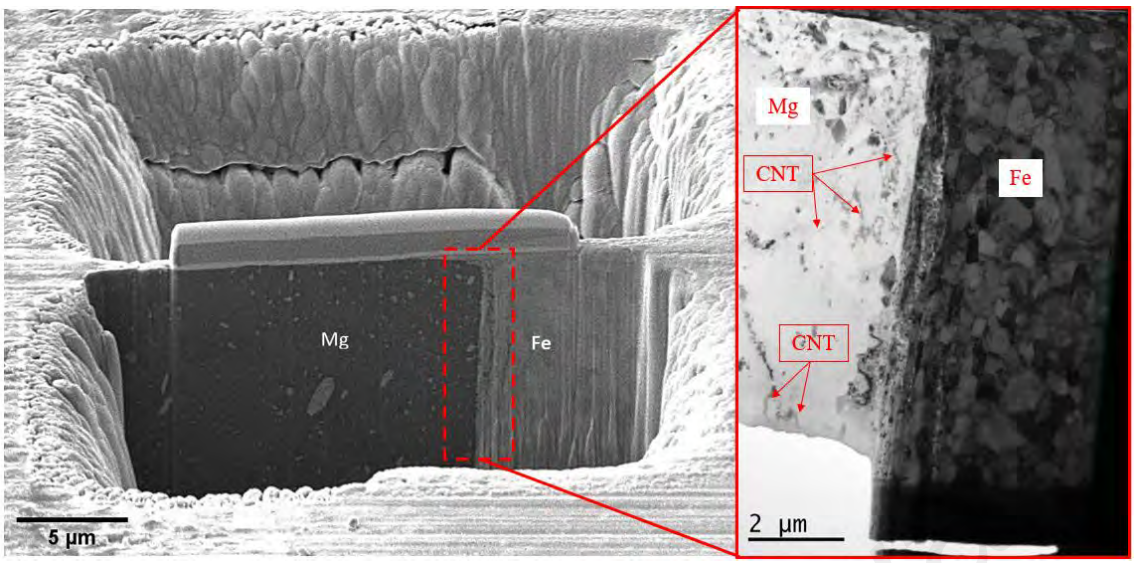

Figure 4.5 Overview of thin lamella obtained from Cu-3 % CNT specimen at traverse speed 30 mm/min.

The magnified TEM image (inset) shows that scattered steel fragments were observed in the Mg matrix and the dispersion of CNT inside the matrix was also detected. It can be seen from the interface that CNT was dispersed in the Mg matrix side. Research on nanoparticle-reinforced metal matrix composites reported that reinforcement particles dispersed inside the grains offers better strengthening efficiency (Xie et al., 2022). When preparing graphene-reinforced aluminum matrix composite by deformation-driven metallurgy, it was found that graphene nanoparticles were homogenously distributed inside the matrix through severe plastic deformation. It was also reported that graphene nanoparticles were mainly dispersed within the grains rather than concentrated at the grain boundaries. Such nanoparticles distribution exhibited Zener pinning effect on the migration of grain boundaries, thereby improving the mechanical properties of the composites. Consistent findings were also observed in this study in which the CNT was successfully dispersed within the Mg matrix rather than agglomerating at the Mg-steel interface. Therefore, the dispersion of CNT in the Mg matrix and its interfacial bonding within the matrix would greatly affect the joint reinforcement efficiency.

TEM images of the interface between Mg and CNT are shown in **Error! Reference source not found.**.

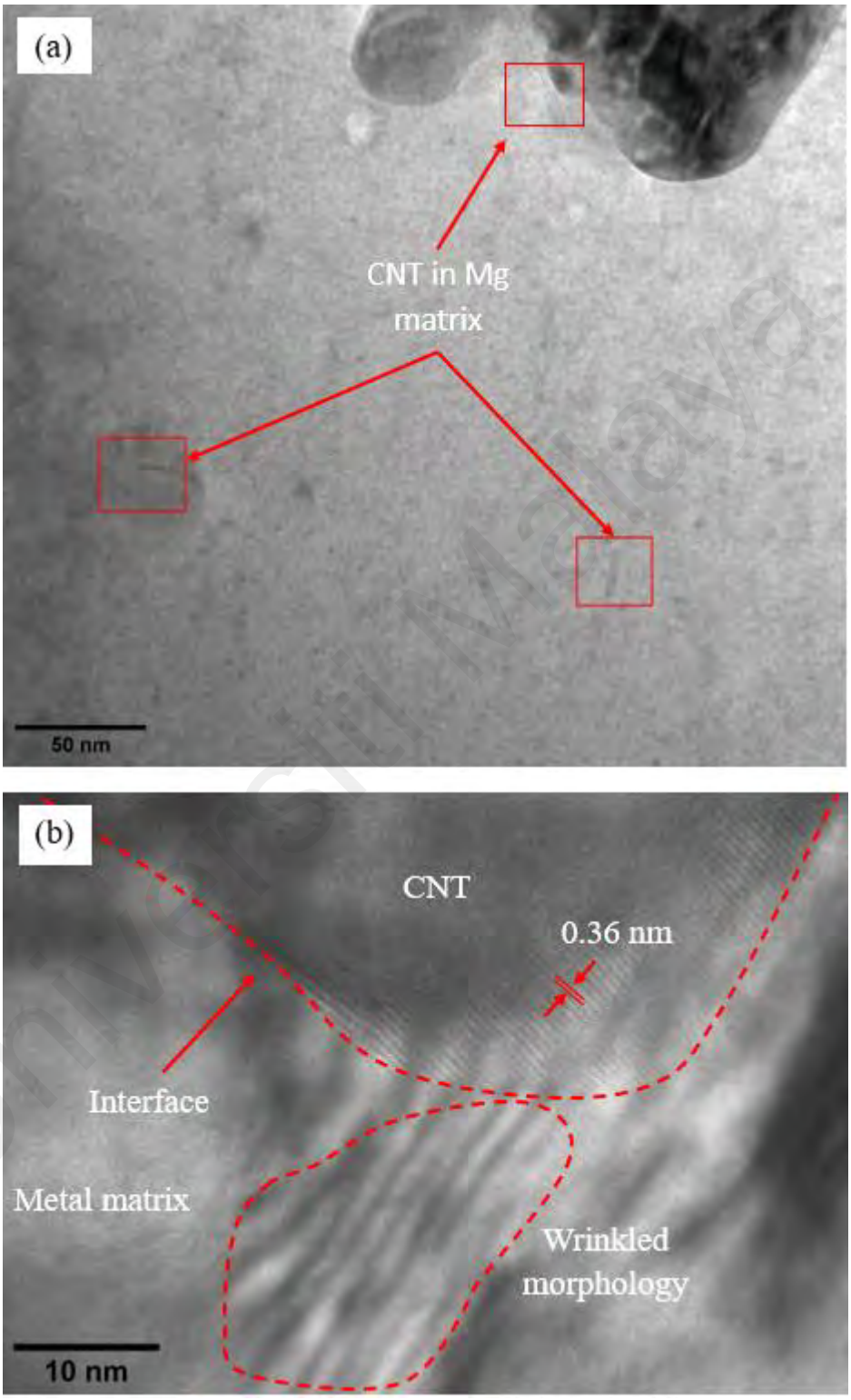

Figure 4.6 TEM images of (a) CNT inside the Mg matrix, (b) wrinkled surface region inside the Mg matrix

Figure 4.6 (a) suggested that CNT was distributed within the Mg matrix. The energy generated through frictional heating during FSA process softened the Mg matrix and experienced plastic flow. This breaks down the CNT's agglomeration and drives the CNT within the vicinity to flow together and eventually be dispersed in the Mg matrix (Zhang et al., 2021). The magnified resolution of the image shown in Figure 4.6(b) depicts the wrinkled morphology, which further indicates the presence of CNT in the surface region. The formation of such wrinkles could be due to the opposite polarity of coefficients of thermal expansion (CTE) between CNT and Mg. Since the CTE of CNT is negative, it causes the horizontal displacement to occur, resulting in the formation of wave-like structure in the matrix (Deng & Berry, 2016).

TEM image in **Error! Reference source not found.** revealed the existence of several d islocations in the Mg matrix near the CNT interface, which implies that good interfacial bonding between CNT and Mg was achieved (Sharma et al., 2020).

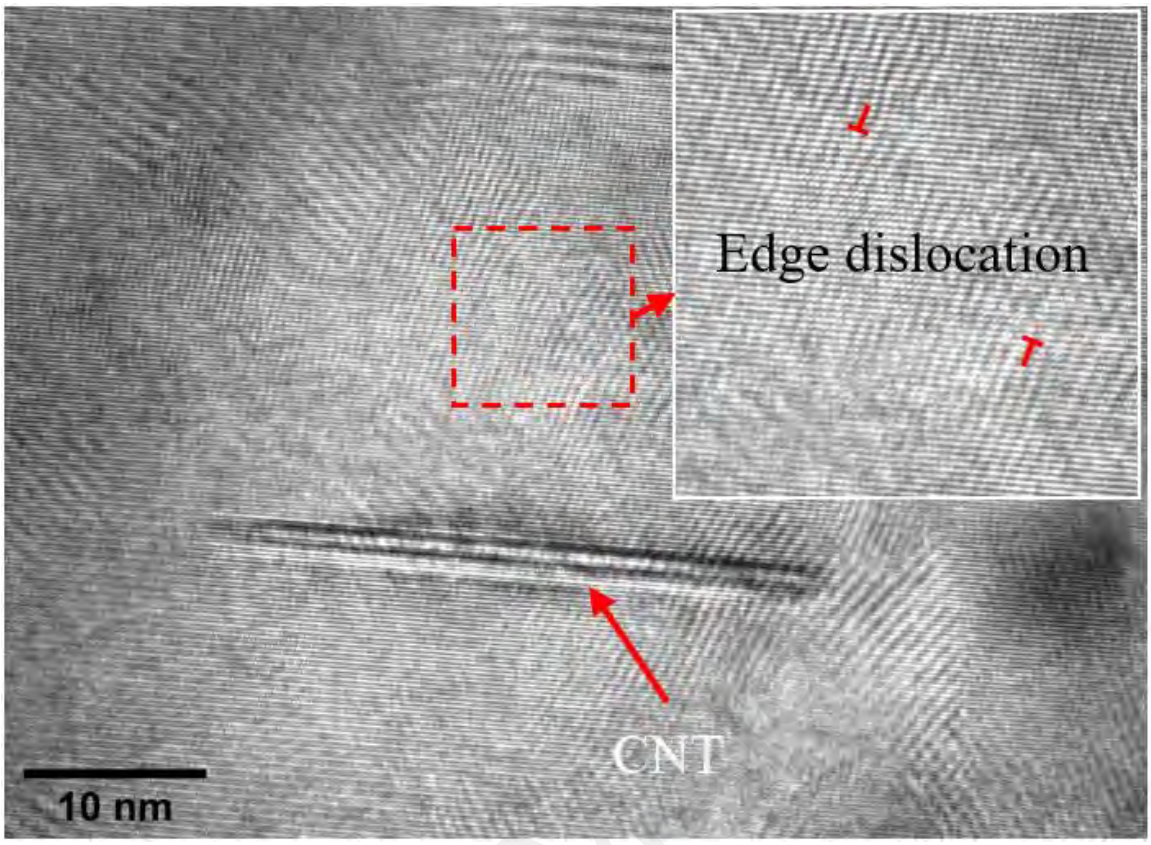

Figure 4.7: Edge dislocations near CNT interface

Embedded CNT in the matrix suppressed the movement of dislocation and promoted localized dislocation aggregation, which accelerated dynamic recrystallization. This means mechanically driven deformation promotes rapid multiplication of necessary dislocations and enables simultaneous nucleation of recrystallized grains (Xie et al., 2021). The role of CNT as reinforcement nanomaterial was clearly demonstrated in Figure 4.3 as the specimens with Cu-CNT additives showed enhanced tensile strength. The improved mechanical properties were attributed to various strengthening mechanisms such as dislocation strengthening by CNT and mismatch of CTE between CNT and Mg (Du et al., 2016; Liang et al., 2017; Mohammed & Chen, 2020). The dispersion of CNT in the Mg matrix could cause the dislocation density in the region to increase. Under the application of external load, the interaction between dislocations in the region with high dislocation density are more, resulting in the improved mechanical properties of the joint. Besides, the existence of CNT in the matrix acts like a particle that

impedes the dislocation movement (Mohammed & Chen, 2020). This is because the strength of CNT is superior as compared to Mg, causing the dislocation shearing more difficult. Besides, opposite polarity of CTE of CNT caused a significant mismatch to that of Mg, which gave rise to the wrinkled surface morphology as presented in Figure 4.6(b). Arsenault & Shi (1986) reported that the generation of such dislocation due to CTE mismatch causes thermal mismatch strengthening in the composite. The mismatch in CTE develops the residual stresses and induces "punching of dislocations" at the surface region. This leads to an increase in the flow stresses, thus increasing the strength of the stir zone material.

4.5 Role of Cu Powder on the IMC Formation at Joint Interface

Observation in Figure 4.8(a) shows the presence of the IMC layer between the Mg-steel interface, with thicknesses ranging from about 0.47 to 0.74 µm. The formation of IMC at the joint interface appeared to be continuous, but its intensity and thickness varied at the different length of the interface.

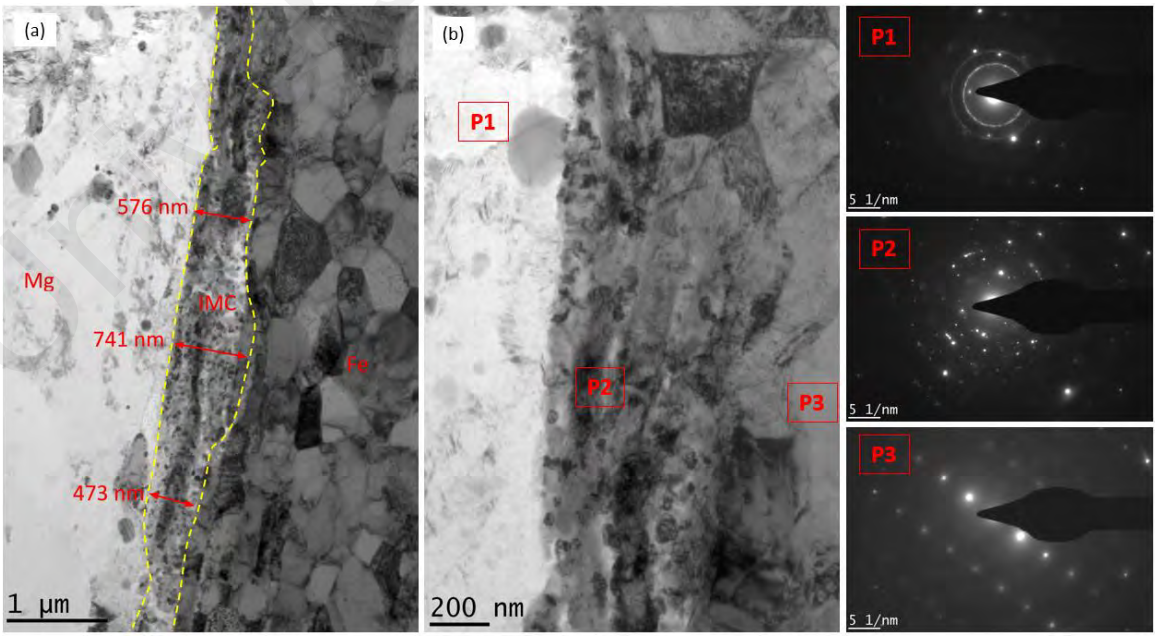

Figure 4.8: TEM images of Mg-steel interface (a) IMC interlayer at the Mg-steel interface, (b) SAED patterns at three different surface regions

Since Mg and steel are immiscible, the addition of Cu in the present experiment served as metallurgical binder to reduce the immiscibility gap between Mg and steel with the help of IMC formation. Kasai et al. (2015) when conducting FSW between Mg alloys and steel suggested that the presence of thin IMC at the interface was essential to obtain Mg-steel joints of high tensile strength. They reported that the Al in Mg facilitated the construction of Al-Fe IMC and improved tensile strength was obtained when the Al content in Mg was increased. In another study, Muhamad et al. (2021) incorporated Al-Mg powder additives to achieve sound joint between Mg alloy and mild steel where he confirmed the presence of IMC at the joint interface which had led to the improved joint strength. Similar findings were also obtained in this study in which a layer of IMC was detected along the interface by TEM analysis. As the Mg-steel transition layer mainly composed of IMC, the dominant presence of Mg_2Cu IMC as demonstrated by XRD results served as strengthening mechanism for Mg-steel joints. This is because the interdiffusion between Mg and Cu elements enhances the metallic interaction between the base metals by enabling a metallurgical bond at the joint interface and therefore improved the joint efficiency.

To determine the crystallinity of IMC and regions of interest near the interface, Selected Area Electron Diffraction (SAED) analysis was conducted. Figure 4.8(b) shows high-magnification TEM image and its corresponding SAED patterns at three different locations in the stir zone. At the Mg side near the interface (P1), discrete bright spots and diffraction rings were both observed, suggesting a polycrystalline structure exists in the region. Meanwhile at the steel side (P3), only discrete bright spots were diffracted. The location of the bright spots was in complete order with consistent pitch distance from each other, which depicts a monocrystalline structure in the region. The result from the SAED pattern at P1 and P3 is consistent with the observation from Figure 4.5 that dispersion of steel fragments and CNT took place inside the Mg side near the interface. At Mg-steel

interface (P2), a random and scattered diffraction ring was observed, which also indicates the characteristic of a polycrystalline structure. The presence of polycrystalline structure in this region implied the interdiffusion of Cu into Mg by means of thermo-mechanical alloying after being subjected to heat and severe plastic deformation. Mg-Cu binary phase diagram as shown in Figure 4.9(a) indicates that two intermetallic phases could be formed between Mg and Cu, which are Mg_2Cu and $MgCu_2$ meanwhile according to Fe-Cu binary phase diagram as shown in Figure 4.9(b), only solid solution could be formed between Fe and Cu (Okamoto & Massalski, 1990; Zhou et al., 2022). Thus, large amounts of Cu particles that were not dissolved in Fe would have more chances to interact with the Mg element, giving rise to the formation of Mg-Cu related IMCs.

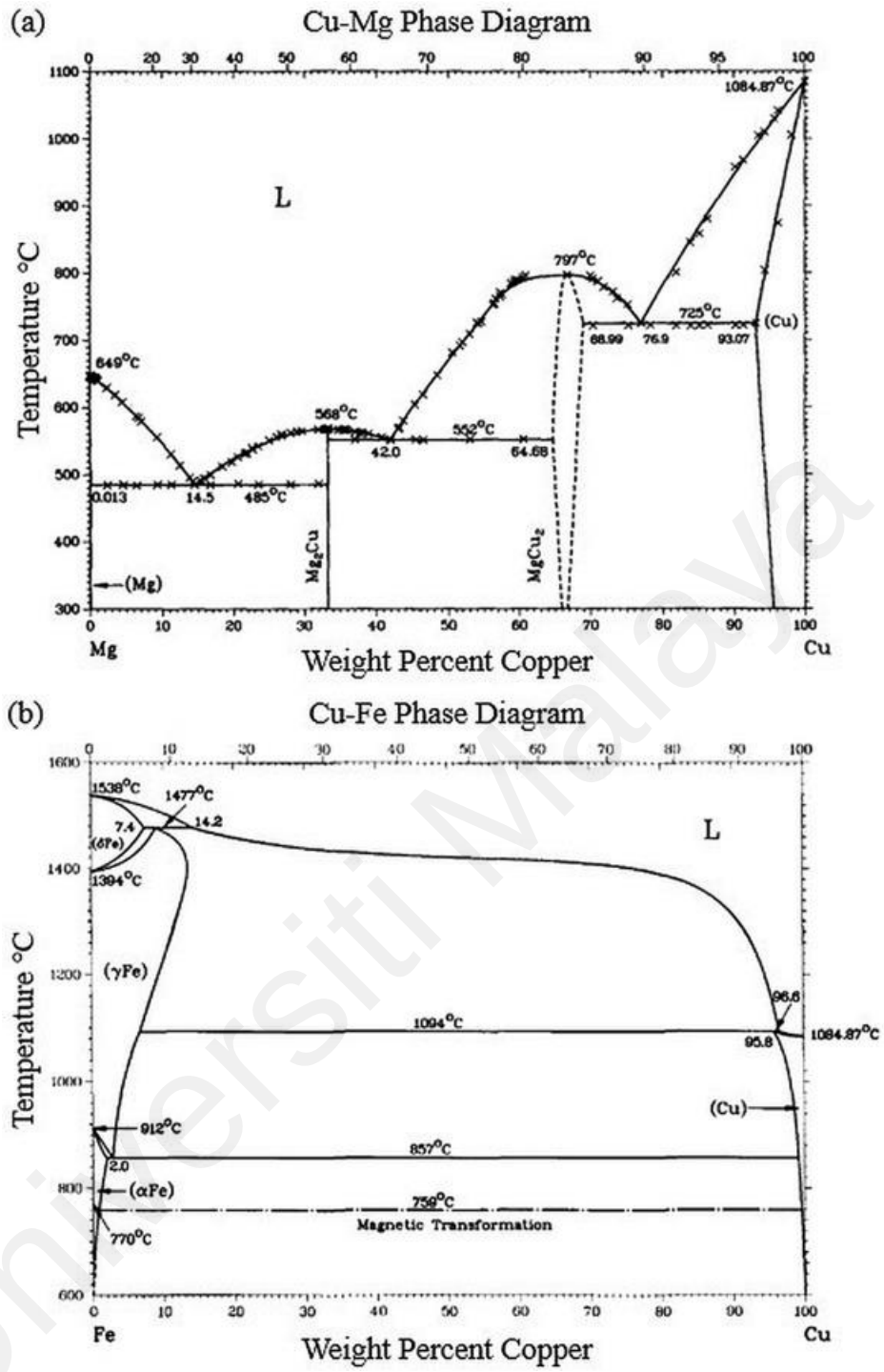

Figure 4.9: (a) Mg-Cu and (b) Cu-Fe binary phase diagrams (Nayeb-Hashemi & Clark, 1984; Okamoto & Massalski, 1990)

The formation of IMCs was further confirmed with XRD results provided in Figure 4.10, that shows the detection of Mg_2Cu and $MgCu_2$ with dominant presence of Mg_2Cu at Mg-steel interface.

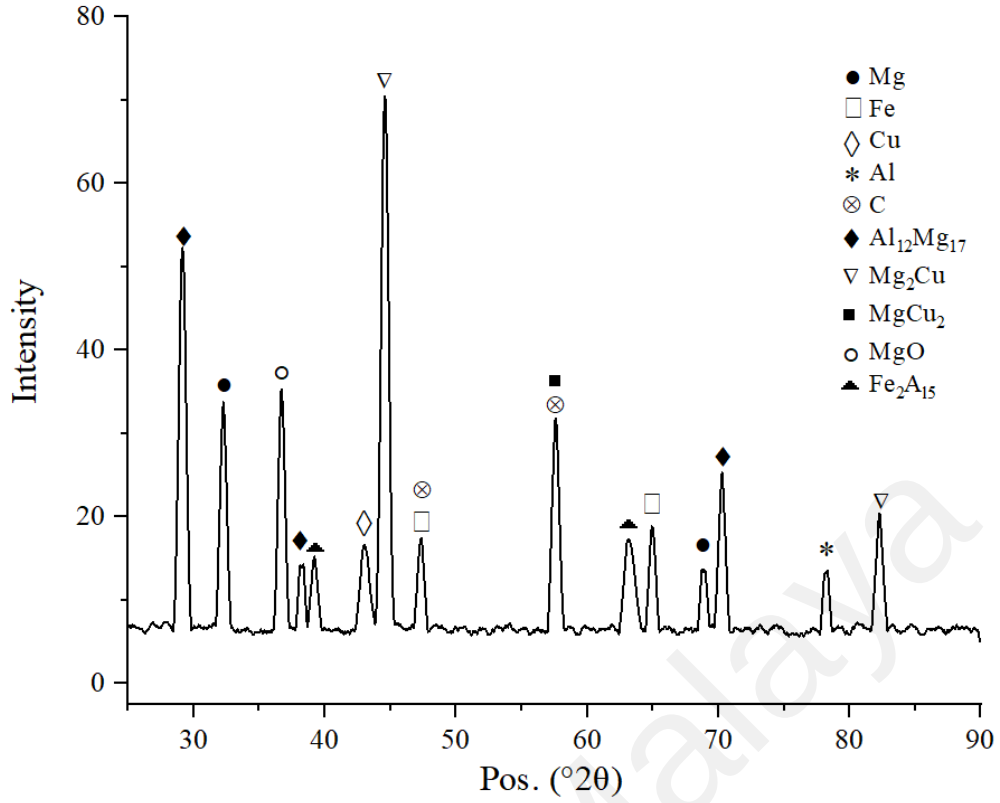

Figure 4.10: XRD pattern of the FSA specimen with Cu- 3 % CNT at traverse speed 30 mm/min

As discussed in the literature, the formation of IMC during dissimilar joining have been identified by two mechanisms. First, IMC can be formed through liquefaction and interaction of dissimilar metals at high temperature. Second, IMC can be generated through diffusion reaction in the solid state. In FSA, component liquefaction was not involved, as the process temperature was lower than the melting point of Cu and Mg alloy. Thus, diffusion reaction was the formation mechanism of IMC in this study. XRD obtained from the Mg-steel composite joint also showed two carbon representative peaks at 47 and 57°, which indicates that CNT was successfully introduced into the metal matrix by FSA. In addition, the formation of Fe_2Al_5 was also detected due to the reaction of Al which present as an alloying element in AZ61 with Fe. Apart from that, the intermetallic phase of $Al_{12}Mg_{17}$ was also detected by XRD along with the intensity of Cu, MgO and other elements from the base materials. The cooling after the FSA process triggered the formation of supersaturated solid solutions of Al in Mg. This caused the undissolved Al

elements in Mg to be precipitated, thus became available for constructing $Al_{12}Mg_{17}$ (DQ et al., 2015).

4.6 Fractographic Observations

Error! Reference source not found. shows the FESEM micrographs of the fracture s urface of the tensile test specimen with Cu-3 % CNT additives produced at traverse speed 30 mm/min. The overview of the fracture region in **Error! Reference source not found.**(a) suggested that there was not much deformation observed and the fracture surface was nearly flat. The stress-strain curve of the Mg-steel joint shown in **Error! R eference source not found.** also did not demonstrate a plastic deformation behavior prior to fracture which suggested a brittle fracture mode. Higher magnification of the fractured region shown in **Error! Reference source not found.**(b) reveals the cleavage structures, thus confirming the brittle behavior of the joint. Generally, the formation of cleavage planes at the fracture surface is attributed to the crack propagation across the crystallographic planes. The observation of such fracture features indicated that the crack initiated at the bottom of the stirred region and propagated across the thickness of the joint. In addition, the fracture position mainly occurred on the Mg side near the interface region. In many cases, severe plastic deformation on Mg alloys results in the formation of basal structure especially in the stir zone due to its hexagonal close-packed (HCP) structure that causes asymmetric mechanical properties (D. Liu et al., 2014; Woo et al., 2006; Xu et al., 2022). Due to this, the grains in the stir zone exhibit different grain orientations than the base metal AZ61 and reduces plastic elongation in the stir zone (Mengran et al., 2020; Zhou et al., 2020). This causes the fracture to appear at the transition zone between Mg base metal and joint interface region during the tensile test. This implied that the Mg region near the interface was the weakest region, therefore determining the excellency of the Mg-steel joint (bin Muhamad et al., 2021; Kasai et al., 2015).

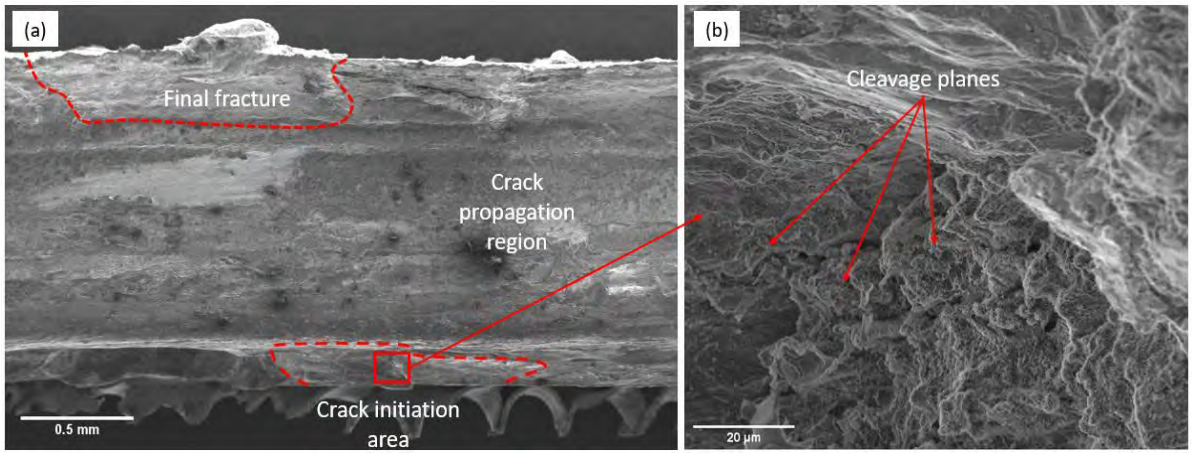

Figure 4.11: FESEM micrographs of the fracture surface: (a) Overview of the fracture surface, (b) Formation of cleavage planes at the crack initiation region

4.7 Hardness Assessments

Error! Reference source not found. shows the microhardness measurement of s pecimens with different additive conditions along the cross-section region.

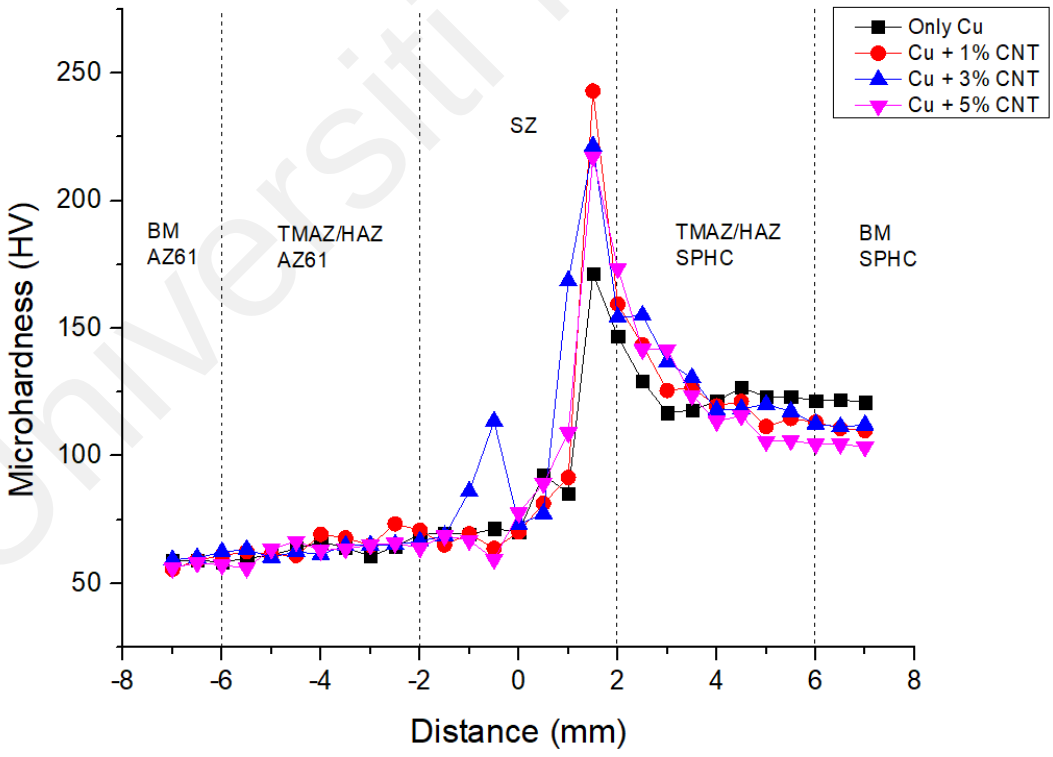

Figure 4.12: Comparison of microhardness values at different additives conditions at traverse speed 30 mm/min

For all the different additives conditions, the hardness measurement achieved its maximum value at about 1.5 mm from the joint center line towards the steel side. The increase in the hardness values in the stir zone near the steel region was mainly attributed to grain refinement. Besides, the effect of CNT on the hardness measurement was clearly demonstrated. The results showed that there exists a significant increase in hardness values of the Mg-steel joints when both Cu and CNT were added as compared to when only Cu powder was added. The present observation agreed with the previous study by Morisada et al. (2006) where he reported that the addition of CNT effectively improved the microhardness of the composites due to the grain refinement and reinforcement of the CNT in the metal matrix. Besides, the addition of CNT established a region with dislocations in the stir zone, which led to greater strengthening effect of the joined material.

CHAPTER 5: CONCLUSIONS

5.1 Conclusions

Dissimilar joint between AZ61 Mg alloy and SPHC mild steel with the incorporation of Cu-CNT additive using the FSA technique was successfully produced. The effects of Cu-CNT addition towards mechanical properties and microstructure characteristics of Mg-steel joint were evaluated. The obtained results from this study are summarized as follows:

1. The addition of Cu-CNT successfully enhanced the tensile strength of FSA joints produced under the optimal traverse speeds. Highest joint efficiency was achieved for specimen with Cu-3 % CNT at 30 mm/min, resulting with 42 % improvement in tensile strength over Mg-steel joint without any additives, as compared to only Cu addition, which showed 13 % improvement in tensile strength. Besides, the incorporation of CNT in the stir zone improved the microhardness. The average hardness increased significantly as approaching the stir zone and reached its maximum value at the steel side near the interface region.
2. TEM analysis of the joint cross-section suggested a good interfacial bonding took place between CNT and Mg matrix through the observation of CNT dispersion inside the Mg matrix near the interface, which reinforced the joint strengthening efficiency. In addition, the dispersion of CNT inside the matrix induced strengthening mechanisms such as high dislocation density and thermal mismatch strengthening that contributed to the improved joining strength.
3. The addition of Cu assisted the formation of IMC along the joint interface was confirmed by TEM analysis, that resulted from the interdiffusion of Cu into Mg element by diffusion reaction through severe plastic deformation. XRD analysis showed the detection of Mg_2Cu and $MgCu_2$ at the Mg-steel interface, respectively.

5.2 Recommendations for future work

To this date, there have not been many studies on the CNT additive in FSA. This study utilized nanomaterial additives of Cu and CNT, where the Cu content was fixed in every experimental condition when joining Mg alloy to steel. Therefore, varied wt.% of Cu in the additive mixture can be adopted in future work to further optimize the mechanical properties of the dissimilar joint. Besides, investigations on the corrosion and tribological properties of CNT added Mg-steel joint can also be considered for future work to ensure broader adoption of the process in various industries.

REFERENCES

Abdollah-Zadeh, A., Saeid, T., & Sazgari, B. (2008). Microstructural and mechanical properties of friction stir welded aluminum/copper lap joints. *Journal of Alloys and Compounds*, *460*(1–2), 535–538.

Akinlabi, E. T. (2010). *Characterisation of dissimilar friction stir welds between 5754 aluminium alloy and C11000 copper*. Nelson Mandela Metropolitan University.

Akinlabi, E. T., Els-Botes, A., & McGrath, P. J. (2011). Effect of travel speed on joint properties of dissimilar metal friction stir welds. *Proceedings of 2nd International Conference on Advances in Engineering and Technology (AET), Uganda*.

Arsenault, R. J., & Shi, N. (1986). Dislocation generation due to differences between the coefficients of thermal expansion. *Materials Science and Engineering*, *81*, 175–187.

Bahrami, M., Helmi, N., Dehghani, K., & Givi, M. K. B. (2014). Exploring the effects of SiC reinforcement incorporation on mechanical properties of friction stir welded 7075 aluminum alloy: fatigue life, impact energy, tensile strength. *Materials Science and Engineering: A*, *595*, 173–178.

bin Muhamad, M. R., Raja, S., Jamaludin, M. F., Yusof, F., Morisada, Y., Suga, T., & Fujii, H. (2021). Enhancements on Dissimilar Friction Stir Welding Between AZ31 and SPHC Mild Steel With Al–Mg as Powder Additives. *Journal of Manufacturing Science and Engineering*, *143*(7).

Bisadi, H., Tavakoli, A., Sangsaraki, M. T., & Sangsaraki, K. T. (2013). The influences of rotational and welding speeds on microstructures and mechanical properties of friction stir welded Al5083 and commercially pure copper sheets lap joints. *Materials & Design*, *43*, 80–88.

Cao, R., Xu, Q. W., Zhu, H. X., Mao, G. J., Lin, Q., Chen, J. H., & Wang, P.-C. (2017). Weldability and distortion of Mg AZ31-to-galvanized steel SPOT plug welding joint by cold metal transfer method. *Journal of Manufacturing Science and Engineering*, *139*(2).

Cao, X., Jahazi, M., Immarigeon, J. P., & Wallace, W. (2006). A review of laser welding techniques for magnesium alloys. *Journal of Materials Processing Technology*, *171*(2), 188–204.

Casalino, G., Guglielmi, P., Lorusso, V. D., Mortello, M., Peyre, P., & Sorgente, D. (2017). Laser offset welding of AZ31B magnesium alloy to 316 stainless steel. *Journal of Materials Processing Technology*, *242*, 49–59.

Chen, Y. C., & Nakata, K. (2010). Effect of surface states of steel on microstructure and mechanical properties of lap joints of magnesium alloy and steel by friction stir welding. *Science and Technology of Welding and Joining*, *15*(4), 293–298.

Deng, S., & Berry, V. (2016). Wrinkled, rippled and crumpled graphene: an overview of formation mechanism, electronic properties, and applications. *Materials Today*, *19*(4), 197–212.

DQ, S., Sun, Y., & ZQ, D. (2015). Effects of Cu addition on microstructure characteristics and tensile behaviors of metal inert-gas arc welded Mg-steel dissimilar joints. *Materials Transactions*, M2015249.

Du, Z., Tan, M. J., Guo, J. F., Bi, G., & Wei, J. (2016). Fabrication of a new Al-Al2O3-CNTs composite using friction stir processing (FSP). *Materials Science and Engineering: A*, *667*, 125–131.

Dziubińska, A., Gontarz, A., Dziubiński, M., & Barszcz, M. (2016). The forming of

magnesium alloy forgings for aircraft and automotive applications. *Advances in Science and Technology. Research Journal*, *10*(31).

Elthalabawy, W., & Khan, T. (2011). Liquid phase bonding of 316L stainless steel to AZ31 magnesium alloy. *Journal of Materials Science & Technology*, *27*(1), 22–28.

Esawi, A. M. K., Morsi, K., Sayed, A., Taher, M., & Lanka, S. (2010). Effect of carbon nanotube (CNT) content on the mechanical properties of CNT-reinforced aluminium composites. *Composites Science and Technology*, *70*(16), 2237–2241.

Esmaeili, A., Rajani, H. R. Z., Sharbati, M., Givi, M. K. B., & Shamanian, M. (2011). The role of rotation speed on intermetallic compounds formation and mechanical behavior of friction stir welded brass/aluminum 1050 couple. *Intermetallics*, *19*(11), 1711–1719.

Gibson, B. T., Lammlein, D. H., Prater, T. J., Longhurst, W. R., Cox, C. D., Ballun, M. C., Dharmaraj, K. J., Cook, G. E., & Strauss, A. M. (2014). Friction stir welding: Process, automation, and control. *Journal of Manufacturing Processes*, *16*(1), 56–73.

Guo, Q., Wang, G., & Guo, G. (2009). *Binary alloy phase diagram of nonferrous metal*. Chemical Industry Press, Beijing.

Gwynne, B., & Lyon, P. (2007). Magnesium alloys in aerospace applications, past concerns, current solutions. *Trienn. Int. Aircr. Fire Cabin Saf. Res. Conf*.

He, B., Cui, L., Wang, D., Liu, Y., Liu, C., & Li, H. (2019). The metallurgical bonding and high temperature tensile behaviors of 9Cr-1W steel and 316L steel dissimilar joint by friction stir welding. *Journal of Manufacturing Processes*, *44*, 241–251.

Horton, P. M., & Allwood, J. M. (2017). Yield improvement opportunities for manufacturing automotive sheet metal components. *Journal of Materials Processing Technology*, *249*, 78–88.

Hou, W., Ding, Y., Huang, G., Huda, N., Shah, L. H. A., Piao, Z., Shen, Y., Shen, Z., & Gerlich, A. (2022). The role of pin eccentricity in friction stir welding of Al-Mg-Si alloy sheets: microstructural evolution and mechanical properties. *The International Journal of Advanced Manufacturing Technology*, *121*(11), 7661–7675.

Hou, W., Shen, Z., Huda, N., Oheil, M., Shen, Y., Jahed, H., & Gerlich, A. P. (2021). Enhancing metallurgical and mechanical properties of friction stir butt welded joints of Al–Cu via cold sprayed Ni interlayer. *Materials Science and Engineering: A*, *809*, 140992.

Huang, Y., Li, J., Wan, L., Meng, X., & Xie, Y. (2018). Strengthening and toughening mechanisms of CNTs/Mg-6Zn composites via friction stir processing. *Materials Science and Engineering: A*, *732*, 205–211.

Inada, K., Fujii, H., Ji, Y. S., Sun, Y. F., & Morisada, Y. (2010). Effect of gap on FSW joint formation and development of friction powder processing. *Science and Technology of Welding and Joining*, *15*(2), 131–136.

Ishikawa, T., Amaoka, K., Masubuchi, Y., Yamamoto, T., Yamanaka, A., Arai, M., & Takahashi, J. (2018). Overview of automotive structural composites technology developments in Japan. *Composites Science and Technology*, *155*, 221–246.

Jana, S., Hovanski, Y., & Grant, G. J. (2010). Friction stir lap welding of magnesium alloy to steel: a preliminary investigation. *Metallurgical and Materials Transactions A*, *41*(12), 3173–3182.

Karthik, G. M., Ram, G. D. J., & Kottada, R. S. (2017). Friction stir selective alloying. *Materials Science and Engineering: A*, *684*, 186–190.

Kasai, H., Morisada, Y., & Fujii, H. (2015). Dissimilar FSW of immiscible materials: steel/magnesium. *Materials Science and Engineering: A*, *624*, 250–255.

Kawajiri, K., Kobayashi, M., & Sakamoto, K. (2020). Lightweight materials equal lightweight greenhouse gas emissions?: A historical analysis of greenhouse gases of vehicle material substitution. *Journal of Cleaner Production*, *253*, 119805.

Khan, N. Z., Siddiquee, A. N., Khan, Z. A., & Shihab, S. K. (2015). Investigations on tunneling and kissing bond defects in FSW joints for dissimilar aluminum alloys. *Journal of Alloys and Compounds*, *648*, 360–367.

Kim, Y. G., Fujii, H., Tsumura, T., Komazaki, T., & Nakata, K. (2006). Three defect types in friction stir welding of aluminum die casting alloy. *Materials Science and Engineering: A*, *415*(1–2), 250–254.

Kostka, A., Coelho, R. S., Dos Santos, J., & Pyzalla, A. R. (2009). Microstructure of friction stir welding of aluminium alloy to magnesium alloy. *Scripta Materialia*, *60*(11), 953–956.

Kulekci, M. K. (2008). Magnesium and its alloys applications in automotive industry. *The International Journal of Advanced Manufacturing Technology*, *39*(9), 851–865.

Kumar, N., Yuan, W., & Mishra, R. S. (2015). Challenges and opportunities for friction stir welding of dissimilar alloys and materials (Chapter 7). *Friction Stir Welding of Dissimilar Alloys and Materials. Elsevier Butterworth-Heinemann*, 123–126.

Kusuda, Y. (2013). Honda develops robotized FSW technology to weld steel and

aluminum and applied it to a mass-production vehicle. *Industrial Robot: An International Journal*.

Lee, W.-B., & Jung, S.-B. (2004). Void free friction stir weld zone of the dissimilar 6061 aluminum and copper joint by shifting the tool insertion location. *Materials Research Innovations*, *8*(2), 93–96.

Liang, J., Li, H., Qi, L., Tian, W., Li, X., Chao, X., & Wei, J. (2017). Fabrication and mechanical properties of CNTs/Mg composites prepared by combining friction stir processing and ultrasonic assisted extrusion. *Journal of Alloys and Compounds*, *728*, 282–288.

Liu, D., Xin, R., Xiao, Y., Zhou, Z., & Liu, Q. (2014). Strain localization in friction stir welded magnesium alloy during tension and compression deformation. *Materials Science and Engineering: A*, *609*, 88–91.

Liu, L., & Qi, X. (2010). Strengthening effect of nickel and copper interlayers on hybrid laser-TIG welded joints between magnesium alloy and mild steel. *Materials & Design*, *31*(8), 3960–3963.

Liu, L., Xiao, L., Feng, J. C., Tian, Y. H., Zhou, S. Q., & Zhou, Y. (2010). The mechanisms of resistance spot welding of magnesium to steel. *Metallurgical and Materials Transactions A*, *41*(10), 2651–2661.

Liu, Y., Zhao, H., & Peng, Y. (2020). Metallurgical reaction and joining phenomena in friction welded Al/Fe joints. *The International Journal of Advanced Manufacturing Technology*, *107*, 1713–1723.

Liyanage, T., Kilbourne, J., Gerlich, A. P., & North, T. H. (2009). Joint formation in dissimilar Al alloy/steel and Mg alloy/steel friction stir spot welds. *Science and*

Technology of Welding and Joining, *14*(6), 500–508.

Massar, M., Reza, I., Rahman, S. M., Abdullah, S. M. H., Jamal, A., & Al-Ismail, F. S. (2021). Impacts of autonomous vehicles on greenhouse gas emissions—positive or negative? *International Journal of Environmental Research and Public Health*, *18*(11), 5567.

Mayyas, A. T., Mayyas, A. R., & Omar, M. (2016). Sustainable lightweight vehicle design: a case study in Eco-Material selection for Body-In-White. In *Lightweight Composite Structures in Transport* (pp. 267–302). Elsevier.

Meng, X., Huang, Y., Cao, J., Shen, J., & dos Santos, J. F. (2021). Recent progress on control strategies for inherent issues in friction stir welding. *Progress in Materials Science*, *115*, 100706.

Meng, X., Xie, Y., Ma, X., Liang, M., Peng, X., Han, S., Kan, L., Wang, X., Chen, S., & Huang, Y. (2022). Towards Friction Stir Remanufacturing of High-Strength Aluminum Components. *Acta Metallurgica Sinica (English Letters)*, 1–12.

Mengran, Z., Yufeng, S., Yoshiaki, M., Kohsaku, U., & Hidetoshi, F. (2020). Quasi-in-situ investigation into the microstructure and texture evolution of pure magnesium during friction stir welding. *Journal of Magnesium and Alloys*, *8*(4), 1071–1083.

Meyer, A. (2012). FSW in automotive mass production–the new Mercedes SL. *Proceedings of the 9th International Symposium on Friction Stir Welding*.

Miao, Y. G., Han, D. F., Yao, J. Z., & Li, F. (2010). Microstructure and interface characteristics of laser penetration brazed magnesium alloy and steel. *Science and Technology of Welding and Joining*, *15*(2), 97–103.

Mishra, M., Iqbal, M. M., Arka, G. N., & Singh, S. (2021). Microstructural and mechanical studies of multi-walled CNTs/Mg composite fabricated through FSP. *Journal of Composite Materials*, *55*(22), 3023–3033.

Mishra, R. S., & Ma, Z. Y. (2005). Friction stir welding and processing. *Materials Science and Engineering: R: Reports*, *50*(1–2), 1–78.

Mofid, M. A., & Loryaei, E. (2019). Investigating microstructural evolution at the interface of friction stir weld and diffusion bond of Al and Mg alloys. *Journal of Materials Research and Technology*, *8*(5), 3872–3877.

Mohammed, S. M. A. K., & Chen, D. L. (2020). Carbon nanotube-reinforced aluminum matrix composites. *Advanced Engineering Materials*, *22*(4), 1901176.

Morisada, Y., Fujii, H., Nagaoka, T., & Fukusumi, M. (2006). MWCNTs/AZ31 surface composites fabricated by friction stir processing. *Materials Science and Engineering: A*, *419*(1–2), 344–348.

Movahedi, M., Kokabi, A. H., Reihani, S. M. S., & Najafi, H. (2012). Effect of tool travel and rotation speeds on weld zone defects and joint strength of aluminium steel lap joints made by friction stir welding. *Science and Technology of Welding and Joining*, *17*(2), 162–167.

Muhamad, M. R., Jamaludin, M. F., Yusof, F., Mahmoodian, R., Morisada, Y., Suga, T., & Fujii, H. (2020). Effects of Al-Ni powder addition on dissimilar friction stir welding between AA7075-T6 and 304 L. *Materialwissenschaft Und Werkstofftechnik*, *51*(9), 1274–1284.

Niu, S., Lou, M., Ma, Y., Yang, B., Shan, H., & Li, Y. (2021). Resistance rivet welding of magnesium/steel dissimilar materials. *Materials Letters*, *282*, 128876.

Ogawa, Y., Ando, D., Sutou, Y., & Koike, J. (2016). A lightweight shape-memory magnesium alloy. *Science*, *353*(6297), 368–370.

Okamoto, H., & Massalski, T. B. (1990). Binary alloy phase diagrams. *ASM International, Materials Park, OH, USA*, 12.

Ouyang, J., Yarrapareddy, E., & Kovacevic, R. (2006). Microstructural evolution in the friction stir welded 6061 aluminum alloy (T6-temper condition) to copper. *Journal of Materials Processing Technology*, *172*(1), 110–122.

Patel, T. A., & Badheka, V. (2022). Rail Welding Technology: Processes and Welding Quality. In *Recent Advances in Mechanical Infrastructure* (pp. 369–381). Springer.

Patel, V. K., Bhole, S. D., & Chen, D. L. (2013). Formation of zinc interlayer texture during dissimilar ultrasonic spot welding of magnesium and high strength low alloy steel. *Materials & Design*, *45*, 236–240.

Patel, V. K., Bhole, S. D., & Chen, D. L. (2014). Characterization of ultrasonic spot welded joints of Mg-to-galvanized and ungalvanized steel with a tin interlayer. *Journal of Materials Processing Technology*, *214*(4), 811–817.

Peng, P., Wang, K., Wang, W., Yang, T., Liu, Q., Zhang, T., Zhang, S., Cai, J., Qiao, K., & Wang, L. (2021). Intermetallic compounds: formation mechanism and effects on the mechanical properties of friction stir lap welded dissimilar joints of magnesium and aluminum alloys. *Materials Science and Engineering: A*, *802*, 140554.

Qi, X., & Liu, L. (2012). Fusion welding of Fe-added lap joints between AZ31B magnesium alloy and 6061 aluminum alloy by hybrid laser–tungsten inert gas welding technique. *Materials & Design*, *33*, 436–443.

Raja, S., Muhamad, M. R., Yusof, F., Jamaludin, M. F., Suga, T., Liu, H., Morisada, Y., & Fujii, H. (2022). Friction stir alloying of AZ61 and mild steel with Al-CNT additive. *Science and Technology of Welding and Joining*, 1–8.

Rao, H. M., Yuan, W., & Badarinarayan, H. (2015). Effect of process parameters on mechanical properties of friction stir spot welded magnesium to aluminum alloys. *Materials & Design (1980-2015)*, *66*, 235–245.

Ritchie, H., & Roser, M. (2020). CO_2 and greenhouse gas emissions. *Our World in Data*.

Saeid, T., Abdollah-Zadeh, A. and, & Sazgari, B. (2010). Weldability and mechanical properties of dissimilar aluminum–copper lap joints made by friction stir welding. *Journal of Alloys and Compounds*, *490*(1–2), 652–655.

Schneider, C., Weinberger, T., Inoue, J., Koseki, T., & Enzinger, N. (2011). Characterisation of interface of steel/magnesium FSW. *Science and Technology of Welding and Joining*, *16*(1), 100–107.

Serrenho, A. C., Norman, J. B., & Allwood, J. M. (2017). The impact of reducing car weight on global emissions: the future fleet in Great Britain. *Philosophical Transactions of the Royal Society A: Mathematical, Physical and Engineering Sciences*, *375*(2095), 20160364.

Shah, S., & Tosunoglu, S. (2012). Friction stir welding: current state of the art and future prospects. *16th World Multi-Conference on Systemics, Cybernetics and Informatics, Orlando, Florida*, 17–20.

Sharma, A., Fujii, H., & Paul, J. (2020). Influence of reinforcement incorporation approach on mechanical and tribological properties of AA6061-CNT nanocomposite fabricated via FSP. *Journal of Manufacturing Processes*, *59*, 604–620.

Sharma, A., Sharma, V. M., & Paul, J. (2020). Fabrication of bulk aluminum-graphene nanocomposite through friction stir alloying. *Journal of Composite Materials*, *54*(1), 45–60.

Singarapu, U., Adepu, K., & Arumalle, S. R. (2015). Influence of tool material and rotational speed on mechanical properties of friction stir welded AZ31B magnesium alloy. *Journal of Magnesium and Alloys*, *3*(4), 335–344.

Singh, V. P., Patel, S. K., Kumar, N., & Kuriachen, B. (2019). Parametric effect on dissimilar friction stir welded steel-magnesium alloys joints: a review. *Science and Technology of Welding and Joining*.

Song, G., Li, T., Yu, J., & Liu, L. (2018). A review of bonding immiscible Mg/steel dissimilar metals. *Materials*, *11*(12), 2515.

Srinivasan, V., Kunjiappan, S., & Palanisamy, P. (2021). A brief review of carbon nanotube reinforced metal matrix composites for aerospace and defense applications. *International Nano Letters*, *11*(4), 321–345.

Sun, Y. F., & Fujii, H. (2011). The effect of SiC particles on the microstructure and mechanical properties of friction stir welded pure copper joints. *Materials Science and Engineering: A*, *528*(16–17), 5470–5475.

Tan, C., Li, L., Chen, Y., & Guo, W. (2013). Laser-tungsten inert gas hybrid welding of dissimilar metals AZ31B Mg alloys to Zn coated steel. *Materials & Design*, *49*, 766–773.

Tan, C. W., Chen, B., Song, X. G., Zhou, L., Meng, S. H., Li, L. Q., & Feng, J. C. (2016). Influence of Al interlayer thickness on laser welding of Mg/steel. *Weld. J*, *95*, 384–394.

Vallentin, D. (2008). Policy drivers and barriers for coal-to-liquids (CtL) technologies in the United States. *Energy Policy*, *36*(8), 3198–3211.

Van Acker, K., Verpoest, I., De Moor, J., Duflou, J.-R., & Dewulf, W. (2009). Lightweight materials for the automotive: environmental impact analysis of the use of composites. *Revue de Métallurgie*, *106*(12), 541–546.

Wang, Q., Zhao, Z., Zhao, Y., Yan, K., Liu, C., & Zhang, H. (2016). The strengthening mechanism of spray forming Al-Zn-Mg-Cu alloy by underwater friction stir welding. *Materials & Design*, *102*, 91–99.

Wang, T., Shukla, S., Gwalani, B., Komarasamy, M., Reza-Nieto, L., & Mishra, R. S. (2019). Effect of reactive alloy elements on friction stir welded butt joints of metallurgically immiscible magnesium alloys and steel. *Journal of Manufacturing Processes*, *39*, 138–145.

Wang, T., Upadhyay, P., & Whalen, S. (2021). A review of technologies for welding magnesium alloys to steels. *International Journal of Precision Engineering and Manufacturing-Green Technology*, *8*(3), 1027–1042.

Wang, X. Y., Sun, D. Q., & Sun, Y. (2016). Influence of Cu-interlayer thickness on microstructures and mechanical properties of MIG-welded Mg-steel joints. *Journal of Materials Engineering and Performance*, *25*(3), 910–920.

Wei, X., Tao, J., Hu, Y., Liu, Y., Bao, R., Li, F., Fang, D., Li, C., & Yi, J. (2021). Enhancement of mechanical properties and conductivity in carbon nanotubes (CNTs)/Cu matrix composite by surface and intratube decoration of CNTs. *Materials Science and Engineering: A*, *816*, 141248.

Woo, W., Choo, H., Brown, D. W., Liaw, P. K., & Feng, Z. (2006). Texture variation and

its influence on the tensile behavior of a friction-stir processed magnesium alloy. *Scripta Materialia*, *54*(11), 1859–1864.

Xie, Y., Meng, X., Chang, Y., Mao, D., Qin, Z., Wan, L., & Huang, Y. (2022). Heteroatom Modification Enhances Corrosion Durability in High-Mechanical-Performance Graphene-Reinforced Aluminum Matrix Composites. *Advanced Science*, *9*(23), 2104464.

Xie, Y., Meng, X., Li, Y., Mao, D., Wan, L., & Huang, Y. (2021). Insight into ultra-refined grains of aluminum matrix composites via deformation-driven metallurgy. *Composites Communications*, *26*, 100776.

Xu, N., Ren, Z., Lu, Z., Shen, J., Song, Q., Zhao, J., & Bao, Y. (2022). Improved microstructure and mechanical properties of friction stir-welded AZ61 Mg alloy joint. *Journal of Materials Research and Technology*, *18*, 2608–2619.

Xue, P., Xiao, B. L., Ni, D. R., & Ma, Z. Y. (2010). Enhanced mechanical properties of friction stir welded dissimilar Al–Cu joint by intermetallic compounds. *Materials Science and Engineering: A*, *527*(21–22), 5723–5727.

Yan, W., Xie, Z., Yu, C., Song, L., & He, H. (2017). Experimental investigation and design method for the shear strength of self-piercing rivet connections in thin-walled steel structures. *Journal of Constructional Steel Research*, *133*, 231–240.

Zhang, S., Chen, G., Qu, T., Wei, J., Yan, Y., Liu, Q., Zhou, M., Zhang, G., Zhou, Z., & Gao, H. (2021). A novel aluminum-carbon nanotubes nanocomposite with doubled strength and preserved electrical conductivity. *Nano Research*, *14*(8), 2776–2782.

Zheng, Y., Pan, X., Ma, Y., Liu, S., Zang, L., & Chen, Y. (2019). Microstructure and corrosion behavior of friction stir-welded 6061 Al/AZ31 Mg joints with a Zr

interlayer. *Materials*, *12*(7), 1115.

Zhou, M., Chen, G., Wu, J., Liu, Q., Lei, B., Gao, Y., Liu, Y., Zhang, S., & Shi, Q. (2022). The Cu/Fe magnetic yoke with novel interface and excellent mechanical properties by friction stir welding. *Science and Technology of Welding and Joining*, 1–14.

Zhou, M., Morisada, Y., & Fujii, H. (2020). Effect of Ca addition on the microstructure and the mechanical properties of asymmetric double-sided friction stir welded AZ61 magnesium alloy. *Journal of Magnesium and Alloys*, *8*(1), 91–102.